



Lawrence Berkeley Laboratory

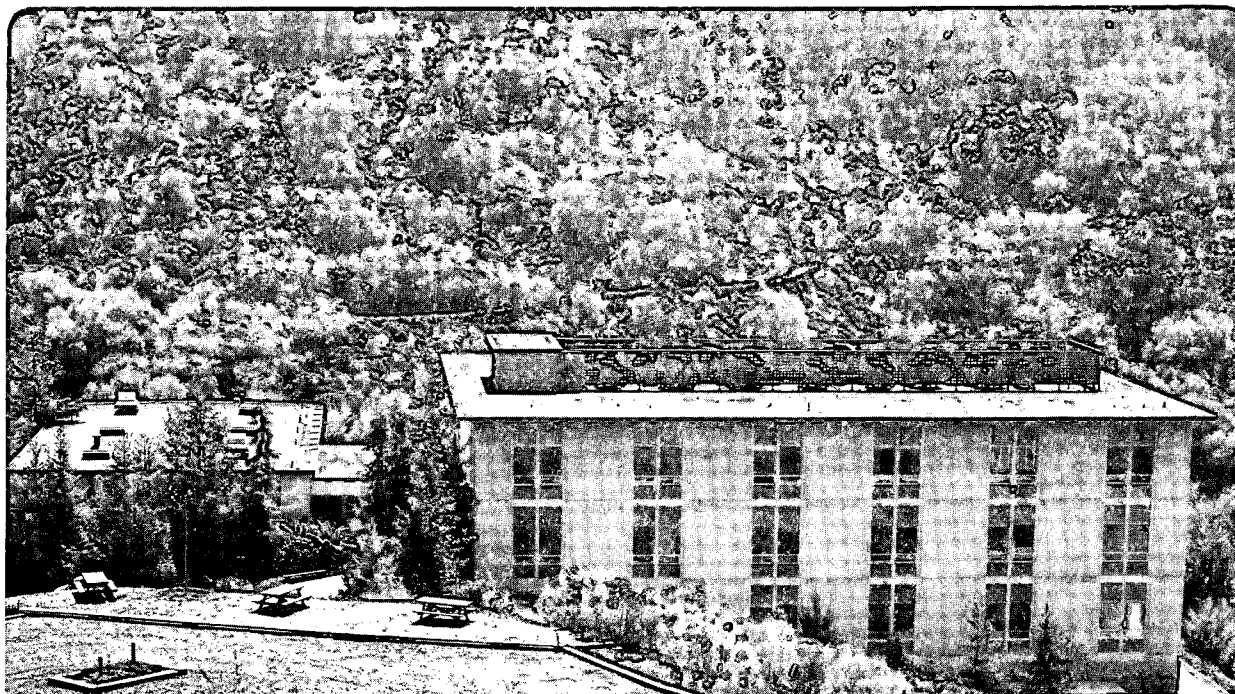
UNIVERSITY OF CALIFORNIA

Materials Sciences Division

The Effect of Surface Morphology on the Friction of Electrogalvanized Sheet Steel in Forming Processes

P.N. Skarpelos
(M.S. Thesis)

December 1993



Prepared for the U.S. Department of Energy under Contract Number DE-AC03-76SF00098

LOAN COPY
Circulates
for 4 weeks
Bldg. 50 Library.

LBL-35038

Copy 2

DISCLAIMER

This document was prepared as an account of work sponsored by the United States Government. Neither the United States Government nor any agency thereof, nor The Regents of the University of California, nor any of their employees, makes any warranty, express or implied, or assumes any legal liability or responsibility for the accuracy, completeness, or usefulness of any information, apparatus, product, or process disclosed, or represents that its use would not infringe privately owned rights. Reference herein to any specific commercial product, process, or service by its trade name, trademark, manufacturer, or otherwise, does not necessarily constitute or imply its endorsement, recommendation, or favoring by the United States Government or any agency thereof, or The Regents of the University of California. The views and opinions of authors expressed herein do not necessarily state or reflect those of the United States Government or any agency thereof or The Regents of the University of California and shall not be used for advertising or product endorsement purposes.

Lawrence Berkeley Laboratory is an equal opportunity employer.

DISCLAIMER

This document was prepared as an account of work sponsored by the United States Government. While this document is believed to contain correct information, neither the United States Government nor any agency thereof, nor the Regents of the University of California, nor any of their employees, makes any warranty, express or implied, or assumes any legal responsibility for the accuracy, completeness, or usefulness of any information, apparatus, product, or process disclosed, or represents that its use would not infringe privately owned rights. Reference herein to any specific commercial product, process, or service by its trade name, trademark, manufacturer, or otherwise, does not necessarily constitute or imply its endorsement, recommendation, or favoring by the United States Government or any agency thereof, or the Regents of the University of California. The views and opinions of authors expressed herein do not necessarily state or reflect those of the United States Government or any agency thereof or the Regents of the University of California.

**THE EFFECT OF SURFACE MORPHOLOGY
ON THE FRICTION OF ELECTROGALVANIZED SHEET STEEL
IN FORMING PROCESSES**

Peter N. Skarpelos

Department of Materials Science and Mineral Engineering
University of California

and

Center for Advanced Materials
Materials Sciences Division
Lawrence Berkeley Laboratory
University of California
Berkeley, CA 94720

December 1993

This work is supported by the Director, Office of Energy Research, Office of Basic Energy Science, Materials Sciences Division of the U.S. Department of Energy under Contract No.

DE-AC03-76F00098

TABLE OF CONTENTS

List of Tables	iv
List of Figures	iv
Acknowledgements	vi
Introduction	1
Background	1
Previous Research	2
Objective	4
Method	4
Experimental Procedures	5
Drawbead Simulator Tests	5
Sample Preparation	6
Area Fraction Deformed Measurements	9
Surface Topography	10
Profile Analysis	11
Experimental Results	13
Commercial Samples	13
Single Value Parameters	13
Bearing Area Curves	14
Power Spectra	15
Area Fraction Deformed	15
Laboratory Samples	16
Change of Morphology by Coating	16
Directionality of Surface Morphology	17
Relationship Between Friction and Surface Parameters	17
Discussion	19
Analysis of Friction in Drawbead Simulator Test	19
Commercial Sample Analysis	20
Laboratory Coated Sample Analysis	22
Summary and Conclusion	24
Tables	25
Figures	26
References	36
Appendix A	40
Appendix B	57
Appendix C	62

LIST OF TABLES

- Table 1: Correspondence of single value surface parameters with coefficient of friction (μ_{DBS}) for the commercial samples. Dual action press used in metal forming, from [36].
- Table 2: Comparison of single value surface parameters before and after the application of the electrogalvanized coating.
- Table 3: Comparison of surface parameters measured in the rolling and transverse directions along the surface of the commercial samples.

LIST OF FIGURES

- Figure 1: Dual action press used in metal forming, from [36].
- Figure 2: Geometry of the one-sided Drawbead Simulator (DBS) test, from [3].
- Figure 3: Method of distinguishing deformed from non-deformed areas in the area fraction measurement.
- Figure 4: BAC curves (Bearing Area vs. Volume Removed) for commercial samples. Samples which exhibit lower friction tend to have flatter BAC's, corresponding to higher R_a .
- Figure 5: BAC curves (Bearing Area vs. Volume Removed) for commercial samples, before and after deformation during DBS test. After undergoing the deformation in the DBS test, all sample surface's BACs shifted towards a middle value; the rougher specimens were smoothed and the smoother samples were roughened.
- Figure 6: Power spectra of four commercial samples, F18 and R18 exhibit low friction in the DBS test, R1 and F22 exhibit high friction. Higher roughness (more area under the spectrum) corresponds to lower friction (F22, R1). If the roughness is distributed to shorter wavelengths, as with F22, the overall roughness does not need to be as great to produce low friction. R18 has the same roughness as F22, but since it is concentrated in the longer wavelengths, it is not as effective.
- Figure 7: Area fraction deformed as a function of coefficient of friction in the Drawbead Simulator test (μ_{DBS}), a) Commercial samples; b) Lab coated samples
- Figure 8: Longitudinal and transverse power spectra from a lasertex sample.
- Figure 9: Deformed area showing the persistence of the micro-roughness in valleys (XBB891-318).
- Figure 10: Deformed surface showing area where lubricant was trapped (XBB880-11499).
- Figure A1: Power Spectra from commercial specimen F14: (a) traces in rolling direction; (b) traces in transverse direction.
- Figure A2: Power spectra of commercial specimen F22: (a) traces in rolling direction; (b) traces in transverse direction.

- Figure A3: Power spectra of commercial specimen RLO: (a) traces in rolling direction; (b) traces in transverse direction.
- Figure A4: Power spectra of commercial specimen R1: (a) traces in rolling direction; (b) traces in transverse direction.
- Figure A5: Power spectra of commercial specimen R18: (a) traces in rolling direction; (b) traces in transverse direction.
- Figure A6: Power spectra of commercial specimen R3706: (a) traces in rolling direction; (b) traces in transverse direction.
- Figure A7: Power spectra of commercial specimen USX: (a) traces in rolling direction; (b) traces in transverse direction.
- Figure A8: Power spectra of commercial specimen F5: (a) traces in rolling direction; (b) traces in transverse direction.
- Figure A9: Power spectra of commercial specimen RC: (a) traces in rolling direction; (b) traces in transverse direction.
- Figure A10: Power spectra of commercial specimen F18: (a) traces in rolling direction; (b) traces in transverse direction.
- Figure A11: Power spectra of commercial specimen VR410: (a) traces in rolling direction; (b) traces in transverse direction.
- Figure A12: Power Spectra from laboratory coated specimen Laser 1: (a) uncoated, traces in rolling direction; (b) coated, traces in rolling direction; (c) coated, traces in transverse direction.
- Figure A13: Power Spectra from laboratory coated specimen Laser 2: (a) uncoated, traces in rolling direction; (b) coated, traces in rolling direction; (c) coated, traces in transverse direction.
- Figure A14: Power Spectra from laboratory coated specimen Shot Blast 1: (a) uncoated, traces in rolling direction; (b) coated, traces in rolling direction; (c) coated, traces in transverse direction.
- Figure A15: Power Spectra from laboratory coated specimen Shot Blast 2: (a) uncoated, traces in rolling direction; (b) coated, traces in rolling direction; (c) coated, traces in transverse direction.
- Figure A16: Power Spectra from laboratory coated specimen EDT 1: (a) uncoated, traces in rolling direction; (b) coated, traces in rolling direction; (c) coated, traces in transverse direction.
- Figure A17: Power Spectra from laboratory coated specimen EDT 2: (a) uncoated, traces in rolling direction; (b) coated, traces in rolling direction; (c) coated, traces in transverse direction.
- Figure B1: Calculation of the Amplitude Density Function (ADF) from a profile.

ACKNOWLEDGMENTS

I first wish to thank Ford Motor Co., Rouge Steel Co., and LTV Steel Co. for providing funding, material and facilities for this work, and Steven Shaffer for introducing me to this subject and guiding me in my early investigations. Without their help this work would not have been possible.

In addition this work was supported by the Director, Office of Energy Research, Office of Basic Energy Science, Materials Sciences Division of the U.S. Department of Energy under the Contract No. DE- AC03-76 SF00098

I would like to thank Wendy Nojima for her help with SEM work and for many discussions about our work, and Mark McCormick and Zequin Mei, who helped me with my programming and with the analysis of the data the computer spits out.

I cannot express enough my thanks to Bill Morris for his constant support throughout my graduate work.

Finally I would like to thank Linda Schmidt for doing everything from cooking for me to proofreading this thesis and making it more readable than my usual science babble, and my parents for giving me the confidence to finish what I've started no matter how daunting it may seem.

INTRODUCTION

BACKGROUND

Electrogalvanized (EG) zinc coatings are increasingly being applied to sheet metal used in automotive body panels to improve corrosion resistance [1,2], and therefore enhance the lifetime of vehicles. EG steel is essentially the same low carbon steel as was previously used for automotive body panels, but with the addition of a 5 to 10 μm thick electrodeposited zinc coating on one or both sides of the sheet. The zinc layer does not significantly alter the mechanical properties of the underlying base metal [3], but does change forming, welding and painting properties of the sheet, and thereby introduces difficulties into the vehicle manufacturing process. The forming problems are twofold. First, the zinc galvanizing layer increases the friction between the workpiece and the tooling during forming [4]. Second, the frictional properties of EG steel can vary significantly from one steel manufacturer to another, and even from lot to lot from a single steel company [3]. To improve the capability of automobile manufacturers to utilize EG sheet steel in vehicle manufacture, it is necessary to have an understanding of the metallurgical properties which affect friction during forming, and to provide reliable specification, inspection and quality control procedures.

The existence of friction in the forming process is not a problem. In fact, friction is necessary in sheet metal forming operations, as it is used to generate restraining forces which control the flow of material into the dies which give the desired shape to parts. However, too much friction can result in splitting or tearing of the sheet, usually at the die radius, or in the region between the binder and the punch (Figure 1). Too little friction allows too much material to flow into the die and causes wrinkling of the sheet. The variability of the frictional properties of EG steel is therefore an important problem for manufacturers.

Using a very thick layer of lubricant to cover the surface and prevent any metal-to-metal contact between the workpiece and tooling would effectively remove the effect of the workpiece surface, however this is not a practical solution to the problem since subsequent to the forming process a part must be cleaned of the lubricant for welding and painting processes. A heavy layer of lubricant would thus cause further problems beyond the forming process.

Measuring frictional properties of a material always involves the conditions under which the friction occurs; the material sliding against the test material, the geometry of contact, the conditions of the surfaces, and the speed of the relative motion of the sliding bodies all affect the frictional properties of a material [5-13]. Therefore many tests have been devised and used to measure these properties for all types of engineering applications. For sheet metal forming operations there are numerous standard tests employed to gauge the frictional properties of materials. These tests range from those that model actual forming process to those that simply slide a test piece over a flat surface of the tooling material. The former tend to convolve the bulk and surface properties but utilize a test geometry as close as possible to that found in the production shops. The latter separate out the surface interaction, but generally at the expense of having a geometry that is not as representative of the actual forming processes modeled. Data obtained from any test must be viewed with consideration of the type of test performed.

PREVIOUS RESEARCH

Though the EG zinc layer on the steel does not change the bulk mechanical properties of the sheet, it does have an effect on how the surface interacts with its tribological environment. The zinc layer has a lower hardness than the underlying steel and has an anisotropic (hexagonal close-packed) crystal structure, unlike the cubic structure of the steel. Both of these properties lead to increased deformation of the surface under loading and promotion of transfer of metal to the opposing surface during deformation [14-22]. The anisotropy of the zinc layer indicates that the friction of a coated

surface should be dependent on the crystallographic texture of the zinc layer. This crystallographic texture is a product of the many variables of the coating process [3]. The lower hardness of the zinc layer would not show the same dependence on these coating process parameters.

Shaffer [3] has shown that the crystallographic texture of the galvanized coating has only secondary importance in the frictional properties of EG sheet steel since all initial textures transformed during the testing to a single texture by either a twinning or recrystallization mechanism. This suggests that the hardness of the coating is the dominant property of the coating affecting friction. Nakamura et al [23] studied the effect of coating type on friction, and their results show that coatings that are alloyed compounds of zinc and either nickel or iron have lower friction in their tests. Since alloyed coatings are harder than pure zinc, this indicates that increasing the hardness of the coating improves the frictional characteristics of the coated sheet steel. However, at present American automobile manufacturers use non-alloyed zinc coatings [4]. Since the hardness of the zinc coating does not change significantly with electrogalvanizing process parameters, only with the composition of the coating, pure zinc EG steels would not be expected to exhibit the variability of frictional properties that are observed with them in stamping plants.

It is possible that the coating accentuates some property of the underlying steel surface which controls the frictional properties of the sheet, rather than affecting the friction independently. Several researchers have found that the surface morphology of the sheet steel is a major factor in the frictional properties of sheet steel [24-35]. In studying uncoated sheet steel, Hilsen and Bernick [24] suggested an optimum surface morphology in the way of a window of peak count and roughness average to minimize friction. Marique et al [25] proposed an anti-galling surface which requires a minimum value of the product of roughness average and mean length of peaks, but only when the roughness of the tooling was comparable to that of the sheet. To date no such correlations have been found to describe zinc-coated sheet steels.

Researchers have found a correlation between the apparent area deformed during sheet metal friction tests and the coefficient of friction measured for both coated and uncoated sheets [3,26]. This area deformed is related to both the hardness of the surface and the original surface morphology of the sheet. If the original morphology of the sheet metal is an important factor in determining its frictional properties, then coating the surface may either change the morphology in some way which affects these frictional properties, or it may accentuate the effect of the initial surface morphology on friction.

OBJECTIVE

The objective of this research is to analyze the role of surface topography on the frictional properties of EG sheet steel as measured with the Drawbead Simulator (DBS) test designed by Harmon Nine of General Motors Co., which is a common friction test used by the automobile industry that correlates well with stamping plant performance [4].

METHOD

This study has two major components. First, a set of commercial samples with a wide range of DBS friction values was analyzed, to see if there was a dominant effect of the surface topography on the frictional properties of commercial EG steels, and find out what properties of the surface morphology if any would correlate to the coefficient of friction measured in the DBS test (μ_{DBS}). Second, a set of similar sheet steels of various surface preparations was coated under the same conditions, so as to isolate the effect of the surface morphology during the DBS test. This, in addition, suggests processing methods which would produce more acceptable sheet steels.

EXPERIMENTAL PROCEDURES

DRAWBEAD SIMULATOR TESTS

The drawbead simulator, developed by Harmon Nine [36] at General Motors, was developed as a means of ranking lubricants used in stamping processes. For this investigation it has been used to compare the frictional properties of different sheet steels. This has been done by choosing a single lubricant to be used for all tests, while varying the sheet metal samples. The lubricant chosen was a SUS 60-viscosity mineral seal oil, which is normally used as a rust preventative oil and has rather poor lubricating properties. This choice was made so that the lubricant would not mask the surface characteristics of the steels as a more effective lubricant might.

The concept of the drawbead simulator test is to pass a sheet through a test geometry simulating the drawbead portion of the die, Figure 2, and to be able to separate the restraining force due to the bending and unbending of the sheet from that due to friction. This is achieved by employing two sets of drawbeads, of identical geometry and material. One set is mounted on roller bearings which reduce the frictional restraint by an order of magnitude, so friction has a negligibly small contribution to the restraining force on the sheet. Thus the measured pulling load is due only to the deformation of the sheet as it is pulled through the geometry of the test. The other set of beads are fixed in position, as opposed to having a rolling surface, and therefore the pulling force measured is the combined restraint due to sliding friction and bending deformation.

In order to compare loads measured in these two test geometries, three identical sheets are pulled through each fixture, for a total of six tests. The pulling and clamping loads of the three test strips are averaged for each drawbead fixture, rolling and fixed. The coefficient of friction for the test is calculated as the difference between the average pulling force in the fixed bead fixture and the roller bead fixture, divided by the average normal

force. Since the normal force is set by the spacing of the drawbead geometry and the yield strength of the sheet metal, this is the same for both fixtures.

To isolate the zinc coated surface of each sheet pulled through the DBS test mechanism, the method used by Shaffer [3] was employed. This method eliminates the surface effect of the non-coated side of the test strip by always using roller fixtures on the double bead side of the test fixture. Thus the only friction involved with the fixed bead is that due to the coated side of the test strip sliding over the single bead. This requires that the coated side of each test strip face the same direction in the test geometry for all tests. With this adaptation, the coefficient of friction is calculated as

$$\mu_{DBS} = \frac{F_{pf} - F_{pr}}{\frac{\pi}{2} F_n} \quad (1)$$

where F_{pf} is the measured force pulling the sheet through the geometry with the fixed beads, F_{pr} is the measured force pulling the sheet through the geometry with the roller beads, and F_n is the normal force applied to the single bead to maintain the test geometry. These forces are indicated in Figure 2.

All DBS testing was performed at Ford Motor Company testing facilities. The samples were lubricated prior to testing by applying the mineral seal oil by brush to reach a saturated lubricated condition on each surface of the sheet. The tests were performed under stroke control at 80 mm/sec pulling speed.

For a more complete description of the DBS test and details regarding the calculation of the coefficient of friction, one is referred to several papers by Harmon Nine and his co-workers at General Motors [36-39].

SAMPLE PREPARATION

The experiments were performed on two sets of specimens. The first was a group of commercial steel specimens from various steel producers which, when tested by Ford Motor Company, were found to exhibit a wide variation in coefficient of friction in the

Drawbead Simulator (μ_{DBS}). The samples are listed in Table 1 in order of increasing values of μ_{DBS} . Each was given a letter designation by Ford to indicate their origin and type of manufacture. These designations are used in this investigation only for the purpose of identification during the comparison of their surface characteristics. These DBS specimens were obtained from Ford after having been tested in their DBS machine. Each was a 30 cm by 5 cm strip. A 12.5 cm section at one end of each specimen was deformed by the drawbeads during the DBS test. This section was used for the analysis of area fraction deformed which is described in the following section. At the other end of the specimen a 2.5 cm section had its surface deformed by the clamp which pulls the specimen through the drawbeads. This section was not used in any of the analyses performed for this study. The area between these two deformed sections is left unchanged by the DBS test. This undeformed area was used for analysis of the surface morphology of the specimens.

To prepare the specimens for subsequent measurements, the specimens were first carefully rolled flat between 2 mm thick cardboard sheets, which protects the surface of the specimens from further deformation. Flat specimens are necessary for the optical techniques used in area fraction deformed measurements, and facilitates surface profilometry. Then the deformed and undeformed sections were separated by a sheet metal shear. The pieces are cleaned for one minute in acetone and then ethanol to remove any dirt and oils remaining on the surface, and then air dried. The deformed sections were then marked with a grid for use in area fraction measurements.

The second set of samples were chosen to examine the effect of different processing of the rolls used in the final, temper roll of the sheet. The temper roll is the final step in the production of sheet metal. This step reduces the thickness of the sheet to its final dimension and embosses the surface of the sheet with the pattern from the rolls for the final surface appearance of the sheet. The pattern is imparted to the rolls by one of several processes. The three most common are shot blasting, electro-discharge texturing

(EDT), and laser texturing. The surface patterns produced by each of these processes are markedly different.

The second set of samples, twelve 50 cm by 65 cm bare steel sheets, were supplied by the LTV Steel Co. Four of these sheets were rolled with laser treated rolls, four were rolled with electro-discharge textured (EDT) rolls, and four were rolled with shot blasted rolls. Of the four sheets from the laser treated rolls, there were two sheets from each of two coils made under the same temper roll conditions by the same laser treated rolls. Sheets from each coil are indicated as Laser1 and Laser2. The four EDT samples also came from two different coils, and the samples of each are indicated as EDT1 and EDT2. (Using sheets from two different coils can provide information about how the surfaces produced during the temper pass changes with roll wear, even if the process parameters were otherwise the same.) The four sheets from the shot blasted rolls were from two coils which had different temper pass conditions. The two sheets from the first roll were reduced 0.2% on the temper pass. Samples from this sheet were labeled Shot1. The two sheets from the second coil were reduced 2% on the temper pass. Samples from this sheet were labeled Shot2. Both coils were produced with the same shot blasted rolls.

The sheets received were nominally 50 cm by 65 cm. These were cut into 50 cm by 15 cm strips on a sheet metal shear for the purpose of applying the electrogalvanized layer using a laboratory coating apparatus at LTV. These samples were analyzed with the profilometer and then sent to LTV's research laboratory for coating with a 10 μm thick coating of pure zinc on a single side of each sample. After the coating was applied, the samples were re-profiled to observe any changes of the surface morphology due to the coating process.

In order to make the most efficient use of a limited supply of material, the 50 cm sheets were then cut into 5 cm by 15 cm inch strips and deburred. Since the length of the area deformed in the DBS test is only 12.5 cm of the specimen, this 15 cm specimen length provided enough material to be drawn through the drawbead fixture, but not enough to

reach the grips which provide the pulling force. A 1 cm wide area on one end of each strip was then sanded to remove the zinc coating. This allowed a 12 cm leader strip of non-galvanized steel sheet to be carefully spot welded to the sheets, without marring the galvanized surface. This leader strip provides enough sheet length to be able to pull the samples through the DBS tester. The samples with the leader welded on were then cleaned with acetone and ethanol and air dried.

After DBS testing the samples, the leader strip was removed and discarded. The deformed samples were then flattened, cleaned, and marked with a grid for area fraction measurements as with the first set of samples.

AREA FRACTION DEFORMED MEASUREMENTS

The measurement of the area fraction deformed during the DBS test was done by contrast imaging on a Nikon microscope fitted with a video camera linked to an IBM personal computer running JAVA image processing software. As shown in Figure 3, the through the lens light source of the microscope illuminates the entire surface, but where the surface has been smoothed due to the DBS deformation, the light reflects directly whereas undeformed areas reflect the light diffusely. The viewed image then appears bright where deformation has taken place and darker where it has not been deformed. By setting contrast levels to single out only the higher brightness pixels, the percentage of the image that is deformed can be determined. By taking a large number of measurements over the entire surface, an average area deformed can be calculated for the specimen. In this study three measurements were taken in each section of an eight section by five section grid covering each specimen, giving 120 measurements per specimen. Each of the three fixed bead DBS specimens was measured in this manner and the results averaged to give the representative value of area fraction deformed.

SURFACE TOPOGRAPHY

Describing the morphology of a surface requires a method for mapping the variation in height of a surface over a prescribed region - the topography - and some method of statistical analysis to reduce this map to a more tractable numerical value or function. This statistical result describes some characteristic of the surface. For example, the difference in height between the highest spot on the surface and the lowest would be a single statistical parameter to describe the roughness, or variation perpendicular to the nominal plane of the surface. Various surfaces can be compared by their corresponding value of a given parameter.

In order to create this topography of a surface many techniques have been devised. The most common is profilometry, which is the recording of the height of a stylus as it traverses in a single line over a surface. This method was originally developed for use with single point tooling machined surfaces, which are characterized long furrows cut into the surface by the tool. A morphology of this type can be described quite completely by a single line trace. Profilometry was the method of surface mapping used in the present experiment.

A stylus measurement device allows measurement of a surface with substantial roughness amplitude yet still obtain a very good spatial resolution. The stylus profiler used in this study has a vertical resolution of $0.01\mu\text{m}$. However, for surfaces not created by single point tool machining, as is the case with sheet metal, a single trace cannot give sufficient information to make valid comparisons. This can be overcome by taking numerous traces covering a small area of the surface in question. These traces can be combined when computing the statistical parameters describing the surface.

In order to perform the statistical calculations on multiple traces and to include any statistical analyses of possible relevance it is necessary to record the surface topography, without filtering, and store the information for later statistical analysis on a computer. This was achieved with a modified Clevite Model 150 SurfAnalyzer, using a $5\mu\text{m}$ radius

diamond stylus tip, and a 25 mg. load. The 5 μm radius tip is smaller than the nominal 10 μm standard, and allows the measurement of some of the finer details of the micro-roughness created by the zinc coating. The 25 mg. load was light enough to prevent the scratching of the relatively soft zinc surfaces. The analog signal produced by the Surfanalyzer was collected through an analog to digital converter and stored on disk by an IBM personal computer for later analysis.

For each specimen, eight parallel profiles of 5 mm length each, spaced 100 μm apart, were taken parallel to the rolling direction, and eight in the transverse direction. The number of profiles taken corresponds to the number needed to arrive at a consistent value for the statistical parameters calculated of the profiles.

PROFILE ANALYSIS

The analysis of the topography measured by the profilometer must in some way distinguish features of the surface of one specimen from another. Surfaces are made up what are termed peaks and valleys in the ANSI/ASME standard [40], which correspond to points of maximum deviations from the nominal surface. The characterization of these peaks and valleys, can be generally put in three categories: roughness, or height of peaks (and corresponding depth of valleys); peak distribution, or spacing of (distance between) peaks and valleys; and shape of peaks and valleys. Numerous statistical parameters used throughout the world are listed in texts on surface metrology [40-43].

For this study, those statistical parameters used were R_a , the arithmetic average of the roughness height variation of the profile, R_{sk} (skewness) which gives a measure of how the points on the surface are distributed about the nominal surface, and R_{ku} (kurtosis) which measures the sharpness of the peaks on the surface, and P_c , the peak count, to measure the spacing of the peaks. Also, to study how the surface supports a load as it is abraded away with testing, the bearing area curve (BAC) was used. In addition, to give a different method of measuring the height and spacing of the peaks on the surface, the fourier power spectrum was employed. This method takes a profile of the surface which is

represented as the variation in height as a function of position, and transforms it into a series of sine waves plotted as amplitude as a function of wavelength. This set of sine waves add to create the original profile. The power spectrum is the plot of the amplitude squared versus wavelength. From the power spectrum the total power (the integral of the spectrum) gives a measure of the roughness height and the median wavelength of the spectrum, λ_m , represents an average spacing of the peaks. Numerous texts on fourier transforms provide detailed discussions on these spectral techniques [44-47]. All of these statistical measures are more thoroughly discussed in Appendix B. The FORTRAN routines employed in the calculation of the statistical parameters is listed in Appendix C.

EXPERIMENTAL RESULTS

COMMERCIAL SAMPLES

Single Value Parameters

The surface parameters for the commercial specimens are listed in Table 1. By measuring the samples in both the rolling and transverse directions it was noted that for single value parameters the value was not dependent on trace direction. Since these sheets were apparently processed with shot blasted rolls this would be expected, as the shot blasting operation is inherently non-directional and results in a fairly gaussian surface morphology in all directions.. The power spectra were also similar when calculated from traces in different directions along the surface of the sheet.

When comparing the parameters to the coefficient of friction measured for these sheets no direct correlation held for a single parameter. As has been suggested by other researchers [31-35], there is the general trend that the sheet surfaces with higher roughness tend to have the lowest friction, but there are several exceptions, most notably the samples labeled RC, R18, and F14. The samples RC and R18 had reasonably high R_a yet still had a moderately high coefficient of friction, though not the highest. In the case of F14 the sample had the lowest R_a of all the samples and one of the lowest coefficients of friction. However, as will be shown in the description of the BAC results, the surface of the F14 sample did not undergo the extensive deformation, while the other samples did, which suggests that the DBS test was not performed in the same way as the other samples.

The samples with low friction also tended to exhibit skewness R_{sk} values close to zero. All the samples with R_{sk} which deviated from zero exhibited high friction. By observing the actual profiles of these specimens one realizes that the R_{sk} values not close to zero indicate a surface with either large plateaus or isolated sharp peaks, either of which

might be expected to generate higher friction during sliding. However it is noted that two samples with higher friction also exhibited skewness close to zero.

The Kurtosis (R_{ku}) was fairly constant at slightly below gaussian for most samples, with the only large deviations from samples which exhibited high friction.

The Peak Count (P_c) varied considerably between samples, but these variation showed no correlation at all with the coefficient of friction for a corresponding sample, no matter how the window height parameter, b , was defined. The P_c was not always as consistent when calculated from profiles in different directions as the other single value parameters, though these variations did not give correspondence between the parameter and frictional properties.

Bearing Area Curves

The BAC's for each of the samples is plotted in Figure 4. Note that instead of plotting versus depth of the profile as is done in [40,41], the bearing area is plotted against the volume of material that would be removed from profile if the surface had been abraded to that height (which is different from the actual deformation which occurs during forming, where the material plastically flows under loading). This was done to indicate the amount of real contact area for a given volume work of deformation. The volume removed is calculated by integrating the change in bearing area from the initial point of contact to the abraded height.

This provides a simple model to compare with the area fraction deformed measurements made of post-friction tested surfaces. The surfaces that give rise to larger area of contact with less deformation of the surface correspond to the samples with higher friction, except for sample F14. When the same plot is made of the post deformation surfaces of the specimens, as in Figure 5, one notes that all the samples have *BAC*'s which shift toward a median curve with the exception of sample F14. As was noted earlier, this result indicated that the surface of the F14 sample did not undergo the extensive

deformation that the other sample surfaces did. It was also noted that this lack of change in the surface held true for the other surface parameters as well.

Power Spectra

The power spectra for each of the samples is shown in Appendix A. One property that is apparent at a glance from these plots is that the surfaces with higher roughness contain more power over the entire spectrum than those with lower R_a . This is born out mathematically as the area under the power spectrum (or the integral of the spectrum) scales with R_a . (The two calculations are analagous, only one is done in fourier space rather than real space.) However, the power spectrum also provides a description of the spacing of the roughness which allows a more complete picture of the types of surfaces which lead to low and high friction. In Figure 6, four power spectra are shown which illustrate how the spacing distribution of roughness correlates to the DBS friction values. The spectrum of sample F18 is indicative of very low roughness and, as would be expected, this sample exhibits high friction. The spectra from the other three samples, F22, R1, and R18, all indicate significant roughness, but sample R18 exhibited high friction unlike the others. The total roughness (area under the spectrum) is the same for samples F22 and R18, but the roughness in both R18 and R1 is more concentrated in the longer wavelengths than in F22. This indicates that the roughness necessary to result in good frictional properties in the DBS test is more effective at shorter wavelengths. If a surface has the majority of its roughness at longer wavelengths, then for lower friction it requires even more roughness to compensate.

Area Fraction Deformed

The area fraction deformed measurements for the commercial samples is shown in Figure 7. Though there is more scatter in these data than in previously reported results, the overall trend of increased area deformed corresponding to higher friction values in the DBS test is the same as in previous work by Shaffer [3]. This indicates that the DBS results are

more dependent on the amount of metal to metal contact during the sliding through the test geometry than on the initial deformation of the surface.

LABORATORY SAMPLES

Change of Morphology by Coating

The surface parameters measured before and after coating of the specimens are listed in Table 2. By analyzing the surface characteristics of the samples before and after coating, one can determine if the coating process changes the surface morphology and thereby the frictional characteristics of the sheets. For the single value parameters the changes were slight between the surfaces of the uncoated and coated steels. The R_a generally decreased slightly upon coating. However most surfaces exhibited no change at all in R_a which suggests that the coating generally conforms to the underlying sheet's morphology without changing it much

The R_{sk} shifts from slightly more plateaus to slightly more valleys in the surface (R_{sk} changes from positive to negative), but this change is negligible compared to the variations seen in the commercial samples.

The R_{ku} also exhibits a shift upon coating which is also small in comparison with the variations observed in the commercial samples. It is interesting to note, though, that in all cases the change is towards a broader gaussian distribution, which means that sharper, more isolated peaks have been smoothed out some. Often in static electroplating processes the peaks on the surface act as sites for faster deposition and therefore the peaks are accentuated.

There was no noticeable change in the power spectra or the Bearing Area Curves upon coating. All of these results suggest that the coating process does not significantly alter the surface morphology of the underlying sheet. This has been observed previously, however, Shaffer [3] noted that for his cadmium doped samples he measured a significant increase in the roughness in the highest concentration of cadmium. In this study the

roughness imparted by the coating is of a sufficiently small scale to not affect the statistical parameters.

Directionality of Surface Morphology

From Table 3 it is clear that for the single value parameters the difference in the direction of the surface profile trace had little effect. This is not true, however, for the power spectra. For the shot blasted surfaces the processing of the roll surface is a random process and should be non-directional. EDT surfaces also tend to be random surfaces. Laser treated rolls, however, impart a definite pattern to the surface of the sheet steel and therefore might be expected to have different values for the parameters of profiles measured in different directions along the surface. The power spectra for the laser textured sheets are significantly different when measured in different directions. In Figure 8 it is clear that in the longitudinal direction there are clear peaks in the power spectrum which indicate a strong pattern in the surface which is not readily apparent in the transverse power spectrum. This result has been found by other researchers as well [48].

In addition, it was noted that the power spectra and the single value parameters for laser textured samples varied with the spacing between traces. It was noted that the surface of the laser textured samples was made up of large, relatively smooth regions with the laser marks in between. Thus if the traces were taken at just the correct spacing the effect of the laser marks could be either exaggerated or minimized, giving a non-representative surface trace. By taking traces at 20 μm spacings, this problem was alleviated.

Relationship Between Friction and Surface Parameters

Table 3 lists the values of each of the single value parameters for the laboratory samples along with their μ_{DBS} values. There was no direct correlation between any one of the single value parameters and μ_{DBS} . For both R_{sk} and R_{ku} , there was no significant difference between any of the laboratory samples, which would indicate that there should not be a variation in friction, yet one is observed. There is a significant variation in R_a for

the laboratory samples. This range of between 0.8 μm and 1.1 μm corresponds to the middle of the range found in the commercial samples. The range of μ_{DBS} measured for the laboratory samples, from .12 to .16 corresponds to the same subset of the commercial samples. However, there is no one to one correspondence between the friction measured for the sample and its R_a .

The power spectra for the laboratory samples tend to contain more of the power in the shorter wavelengths than the commercial samples. But in all cases the area under the spectrum was less than that of the rougher commercial samples. Though the lower friction values were measured for the samples with larger area under the spectra and with the finer spacing of the roughness, the power spectrum still was not sufficient to distinguish between low and high friction in all cases.

For the two shot blasted samples, the power spectra were very similar and yet the sheet which had been subjected to a 2% reduction in thickness on the temper pass had a much higher coefficient of friction than the sheet that had been subjected to a 0.2% reduction. Since the thickness of these sheets were considerably different (0.66mm vs. 0.91 mm respectively) and was the only significant difference between the sheets, it would appear that a large variation in thickness has as pronounced effect on the friction value as the roughness of the surface. This is expected since, as is discussed in the following section, the coefficient of friction is directly related to the actual distance slid across the drawbead during the test. A thicker specimen is stiffer, and does not conform as well to the test geometry, resulting in a lower coefficient of friction .

DISCUSSION

ANALYSIS OF FRICTION IN DRAWBEAD SIMULATOR TEST

In order to discuss the effect of surface morphology on friction it is necessary to analyze the genesis of friction in the DBS test. The test geometry is shown schematically in Figure 2. In passing through this geometry, the surface of the specimen is deformed under the pressure imposed by the bending of the sheet. The real area of contact is initially determined by the elastic stiffness of the sheet. Then this surface is slid along the cylindrical tooling causing further deformation to the surface. Since the forces acting initially to conform the test specimen to the geometry is essentially the same in both the rolling and sliding configurations of the test, this initial deformation contributes only a minor amount to the friction measured by the test. It is the friction generated during the subsequent sliding over the tooling that is the major source measured in the test. This is a significant difference from the strip draw test.

Other researchers have suggested that friction during sliding can be discussed in terms of three modes or components [51]: deformation friction, the friction generated by plastically deforming one or both the contacting surfaces; plowing friction, the generation of friction by asperities in one surface gouging the other in the manner of a machining tool bit; and adhesion friction, the friction generated by the formation of physically adhered (sometimes termed "cold-welded") junctions and their subsequent shearing. Experimental evidence suggests that all three play some role in the friction measured in the DBS test. In Figure 9 it is seen that the large asperities have been deformed during sliding, and, closer inspection of the surface of these deformed asperities reveals smaller furrows indicative of plowing by asperities on the tool surface. Subsequent analysis of drawbeads indicates that for galvanized steels there is often some zinc transfer to the test fixtures. Analysis of the effect of the surface morphology must take each mode of friction into account.

The surface morphology can and does affect each of these modes of friction. The amplitude, shape and spacing of the roughness all affect the slope of the asperities, which has a great effect on the deformation friction as modeled by Green and by other researchers [52-55]. A steeper slope according to these models will lead to increased friction. The amplitude of the roughness as measured by R_a , and, perhaps more importantly, the shape of the asperities as described by the R_{ku} should both tend to increase the slope of the asperities and therefore the friction generated in this mode. Similarly, the size and shape of the asperities will have an impact on the size and number of wear particles generated during sliding. This in turn affects the contribution of the plowing friction. In addition the valleys on the surface of the sheet provide a method of trapping wear particles, which has been shown to significantly reduce effect of plowing.

Since this is a lubricated test, an important property of the surface is how it affects the flow of lubricant. If the lubricant is trapped in small cavities so that it cannot flow out during the deformation, it will support a portion of the load hydrostatically. This would lower the real area of contact, and hence lower both the deformation and adhesion components of friction. A simple view could be that if there were more closely spaced roughness, the lubricant would tend to be trapped between asperities and support more of the load. Other actions of lubricant additives have been studied previously [56] that indicate that formation of boundary layer compounds also lower friction. If this is the case then the effect of surface morphology on the flow of lubricant would have an affect on these processes as well. In this study, however, there were no such additives used, so this would not be expected to affect the results discussed.

COMMERCIAL SAMPLE ANALYSIS

The commercial samples exhibited a very narrow range of values for the R_{ku} and R_{sk} statistical parameters. Most samples had values for these parameters which indicated a surface morphology with very close to a smooth gaussian distribution. Those samples which deviated significantly from these average values exhibited poorer frictional

properties. However, these deviations in R_{sk} and R_{ku} accompanied low roughness amplitude as well, so the significance of these parameters as predictors of frictional properties is not obvious. The roughness amplitude was a better indicator of the frictional properties, as all low friction samples had higher roughness amplitude, with the one exception of sample F14. If the roughness amplitude correlation is true, then this anomalous sample must be accounted for.

As was shown in the BAC plots in Figure 5, the F14 sample was the only curve that did not exhibit a significant change upon deformation. This implies that the sample did not undergo the same amount of deformation during the DBS test as did the rest of the samples. If this is the case, then it is reasonable to expect the sample to show low friction. However, it then suggests that in some way the DBS test was executed in some way different for this sample. For example, if the lubricant used for this sample was not the SUS 60 mill oil, or if the double drawbead spacing was not adjusted correctly to match the thickness of the sample, then the resulting coefficient of friction measured would be comparatively low with respect to the rest of the samples.

As previously noted, high R_a was not sufficient to obtain low friction. From the power spectra one can discern that for the high R_a to be most effective, it must be distributed to shorter wavelengths. For the samples with high roughness mostly in the wavelengths longer than 300 μm , a significantly higher R_a was necessary to give lower friction results. This suggests that there are two ways in which the roughness of the sheet can influence the coefficient of friction in the DBS test. First, if R_a is high enough and is distributed over longer wavelengths, then the wear debris generated by the plowing of the surface become trapped in the large valleys and are therefore less important to the friction generated during sliding. If the roughness is more finely spaced, then the lubricant is trapped in smaller valleys on top of the larger asperities and hydrostatically supports a fraction of the load, thus reducing the effective deformation of the surface and preventing some plowing of the surface.

In Figure 10 one can see areas of sample F22 where plowed layers surround a deformed part of the surface which has not been plowed. The unplowed area still exhibits the original zinc crystal morphology from the coating process. This suggests that the surface was protected by a small trapped area of lubricant. In sample RLO, where the power spectrum was skewed toward the longer wavelengths, this type of protection was not observed, suggesting that some other mechanism was responsible for reducing the friction. Since there was no evidence of wear debris after cleaning the lubricant from the surface for electron microscopy, and the lubricant itself was not analyzed for particle content, it is not possible to tell if there was a trapping of the wear debris by the shorter wavelength roughness. The surfaces of the DBS tooling were analyzed and no zinc transfer was observed. However, for both samples, F22 and RLO, the real area of contact was reduced in some way by what seems to be an interaction with the lubricant.

Emmens [29] suggests that at low pressures, the friction is governed by the flow of lubricant through micro-channels in the rough surface. Wilson [34] also notes that the friction is governed by the entrainment of the lubricant through the test geometry. Shaffer [3] showed that when the micro-roughness was etched from his EG samples that there was increase in the friction in the DBS tests. Schey and Dalton [57] also noted that the small scale roughness on EG sheets makes them have lower friction. In addition, Schey and Dalton stated that the effect of the viscosity of the lubricant was more pronounced with EG steels, indication that the lubricant was trapped by the small scale roughness. The results of the present study indicate that a minimum roughness amplitude is necessary to trap enough lubricant to reduce the metal to metal contact during sliding. In addition, the spacing of that roughness affects how high the necessary amplitude must be to lower friction.

LABORATORY COATED SAMPLE ANALYSIS

The differences in the surface morphology due to the processing of the temper pass rolls do not show a single processing method to be superior to the others. For each of the

EDT, shot blast, and Laser textured rolls, there were samples which exhibited low friction. The surfaces with roughness average of greater than $.8 \mu\text{m}$ had lower friction values. This is slightly lower roughness than was necessary in the commercial samples. However the mean wavelength of the power spectra for the laboratory coated samples with low friction was shorter than for those in the commercial set. This suggests that the micro-roughness imparted during the coating process described by Shaffer [3] is more pronounced in the laboratory coated samples than in the commercial samples. This smaller scale topography, as was noted earlier seems to trap the lubricant and provide a thicker lubricant film.

The one exception to this result is with the shot blast sheet which underwent a 2% reduction during the temper pass. This sheet exhibited higher friction than the other sheets even though its surface topography was nominally the same as that of the shot blast sheet that underwent a 0.2% reduction during the temper pass. This high friction sample was substantially thinner than the other specimens (.66 mm as opposed to .91 mm for the 0.2% reduced sheet and .81 mm for the rest of the sheets) which means that it would conform better to the drawbeads during the DBS test. This would affect the actual contact distance and raise the measured coefficient of friction.

SUMMARY AND CONCLUSION

The effect of the surface morphology on the frictional properties of EG sheet steel in the drawbead simulator test were evaluated for a set of commercially coated steels and a set of laboratory coated steels with underlying surfaces produced by laser textured, shot blast, and electro-discharge textured rolls.

In general, surfaces with higher roughness as described by the R_a parameter measured lower friction in the DBS tests. The requisite roughness amplitude necessary for low friction was moderated somewhat by having a more closely spaced roughness as described by the median wavelength, λ_m , of the power spectrum. This effect is due to interaction with the lubricant by the micro-roughness imparted by the galvanizing process. The lubricant tends to be retained better by the surfaces with the micro-roughness, thereby increasing the amount of elasto- and plasto-hydrodynamic support of the load.

Other variables, such as large variations in thickness of the sheet can mask the effect of the surface by changing the actual distance of sliding contact during the DBS test. For tests where the amount of sliding is similar, the effect of roughness is significant.

The friction measured for EG steels in the DBS test is dominated by deformation of the surface with plowing by the asperities of the tooling adding to that caused by the deformation. The size of the plow marks in the deformed surfaces corresponds to the roughness of the tooling and no significant evidence of wear particles was observed.

TABLES

Sample	μ_{DBS}	R_a	R_{sk}	R_{ku}	λ_m	P_c
F14	0.09 _(+/-0.005)	0.42(μm)	-0.684	3.639	0.178 (mm)	260
F22	0.09	1.28	-0.062	2.192	0.146	419
RLO	0.11	1.28	-0.099	2.363	0.320	246
R1	0.12	1.40	0.210	2.264	0.427	301
R3706	0.12	0.98	-0.217	2.504	0.465	156
R18	0.16	1.12	-0.426	2.317	0.223	380
USX	0.16	0.99	0.345	4.511	0.301	284
F5	0.17	0.54	0.158	2.704	0.256	301
RC	0.17	1.20	0.071	13.657	0.341	166
F18	0.19	0.52	0.896	7.229	0.135	305
VR410	0.19	0.65	-0.263	3.429	0.146	314

Table 1: Correspondence of single value surface parameters with coefficient of friction (μ_{DBS}) for the commercial samples.

Sample	R_a	R_a	R_{sk}	R_{sk}	R_{ku}	R_{ku}	λ_m	λ_m	μ_{DBS}
	bare	coated	bare	coated	bare	coated	bare	coated	
Laser1	0.79	0.86	0.28	0.04	3.63	2.43	0.26	0.24	0.13
Laser2	0.82	0.84	0.35	0.07	2.75	2.25	0.30	0.30	0.15
Shot1	0.72	0.69	0.44	-0.16	3.79	-2.78	0.20	0.11	0.13
EDT1	0.94	0.90	0.44	0.02	3.67	2.69	0.15	0.16	0.14
Shot2	0.78	0.77	0.40	0.16	3.23	3.84	0.14	0.26	0.17
EDT2	0.89	0.90	0.33	-0.03	2.89	2.40	0.14	0.14	0.13

Table 2: Comparison of single value surface parameters before and after the application of the electrogalvanized coating.

Sample	R_a	R_a	R_{sk}	R_{sk}	R_{ku}	R_{ku}	λ_m	λ_m	μ_{DBS}
	Roll	Trans	Roll	Trans	Roll	Trans	Roll	Trans	
Laser1	0.90	0.86	0.09	0.04	2.53	2.43	0.24	0.17	0.13
Laser2	0.83	0.84	0.11	0.07	2.48	2.25	0.30	0.17	0.15
Shot1	0.67	0.69	-0.13	-0.16	2.63	2.78	0.11	0.15	0.13
EDT1	0.90	0.90	-0.02	0.02	2.43	2.69	0.16	0.17	0.14
Shot2	0.72	0.77	-0.04	0.16	2.60	3.84	0.26	0.12	0.17
EDT2	0.90	0.90	-0.05	-0.03	2.41	2.40	0.15	0.15	0.13

Table 3: Comparison of surface parameters measured in the rolling and transverse directions along the surface of the commercial samples.

FIGURES

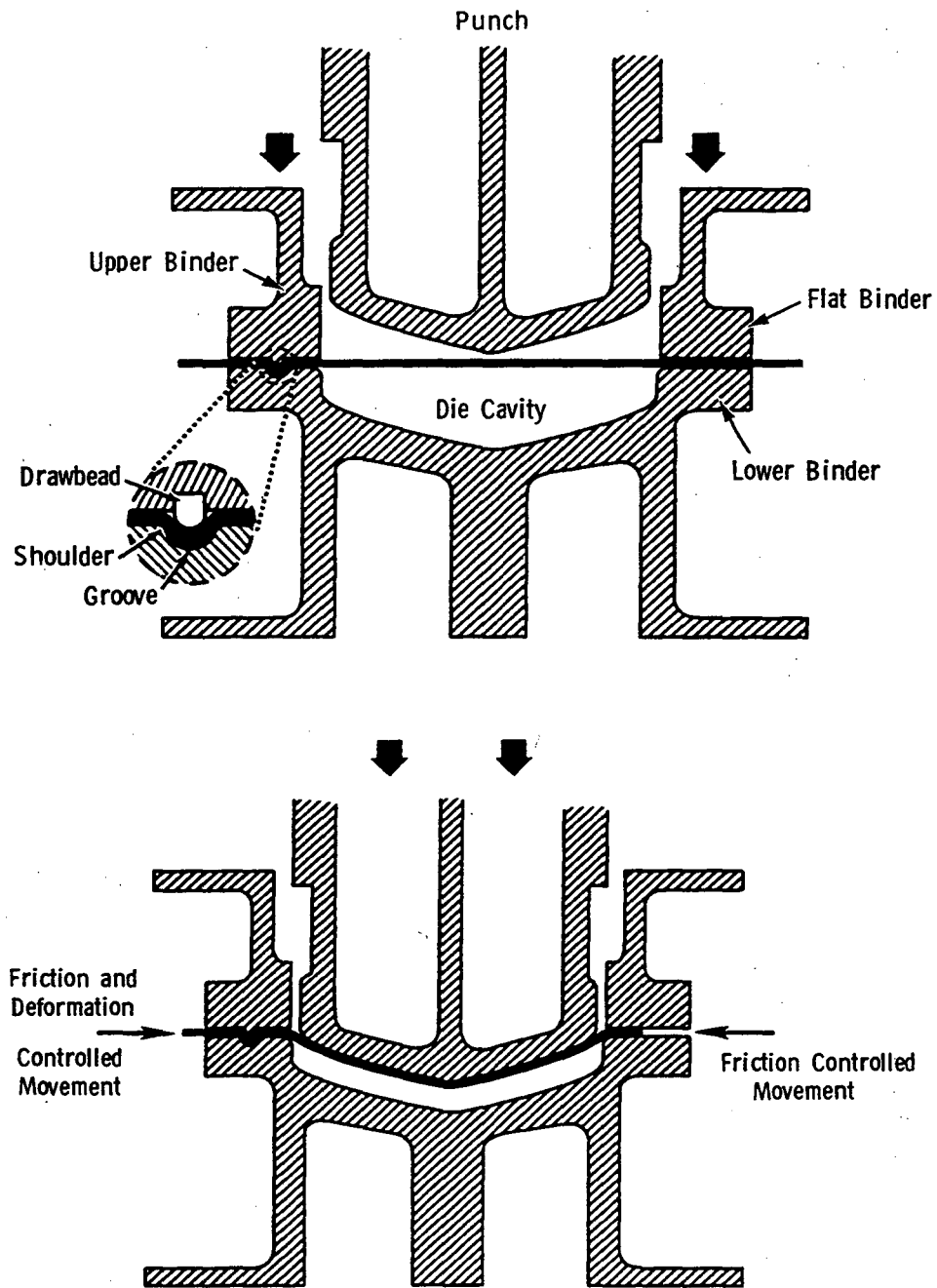


Figure 1: Dual action press used in metal forming, from [36].

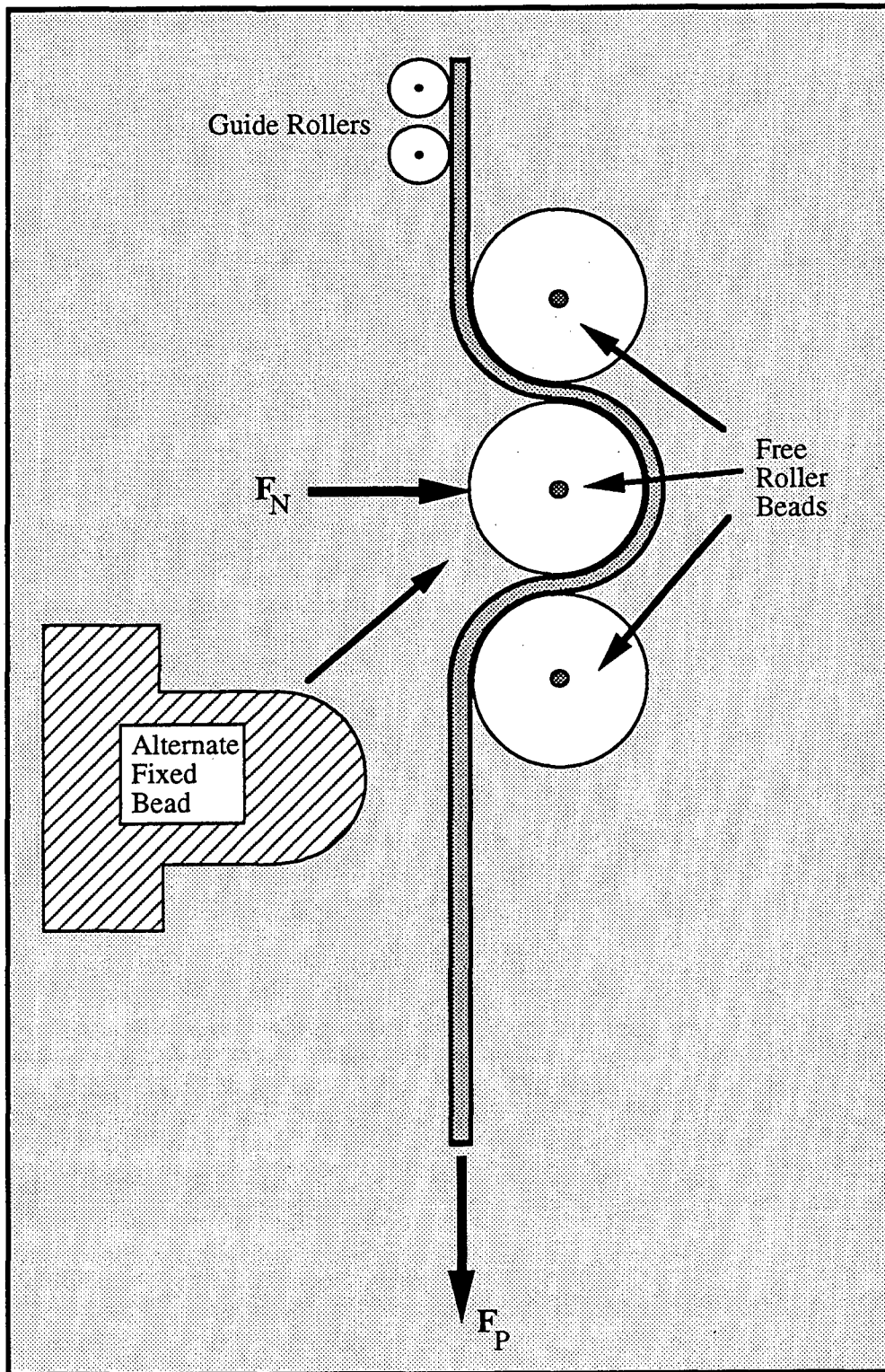


Figure 2: Schematic geometry of the one-sided DBS test, from[3].

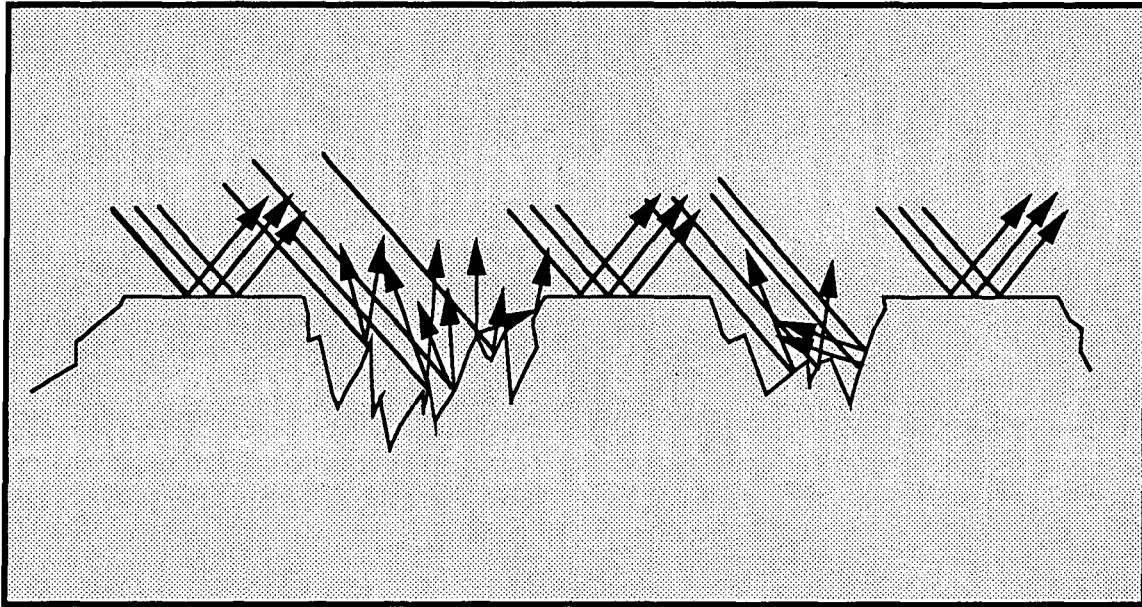


Figure 3: Method of distinguishing deformed from non deformed areas in the area fraction measurement.

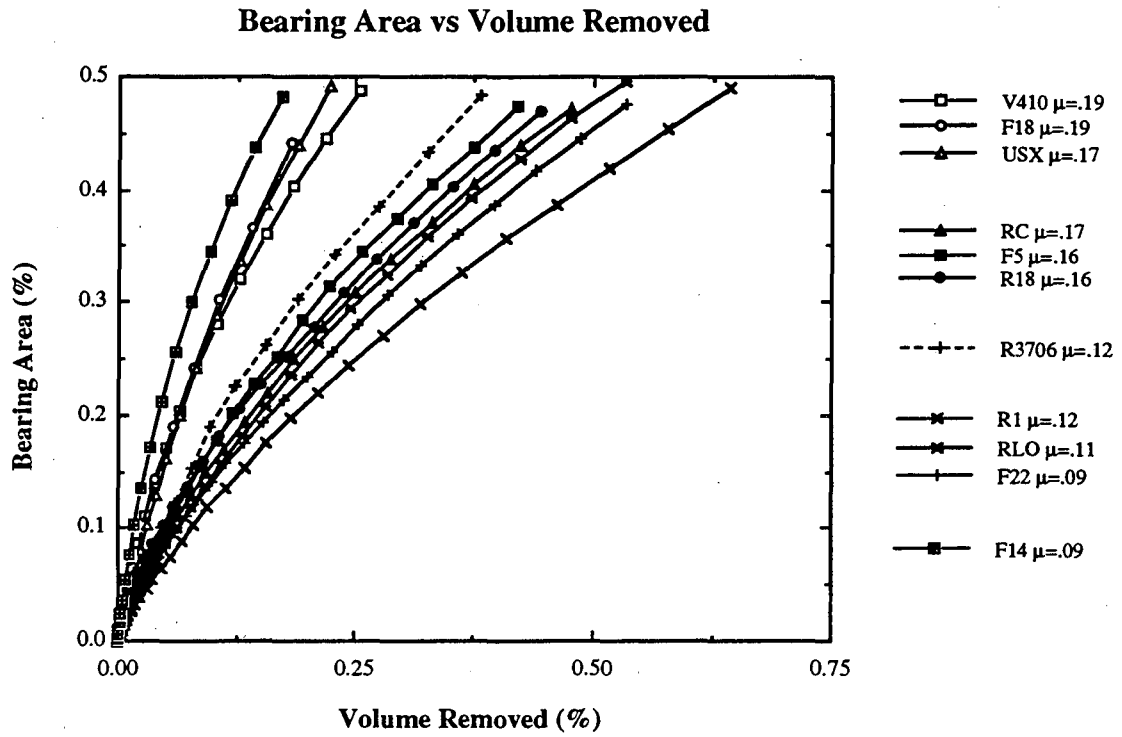


Figure 4: BAC curves for commercial samples. Samples which exhibit lower friction tend to have flatter BAC's, corresponding to higher R_a .

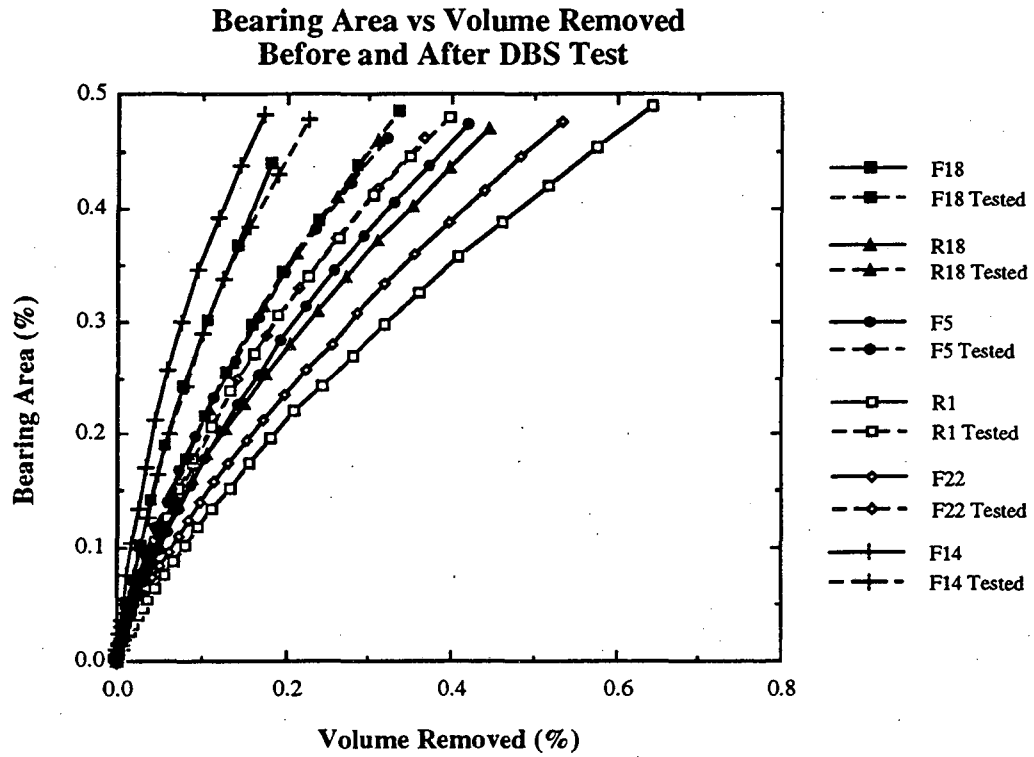


Figure 5: BAC curves for commercial samples before and after the deformation in the DBS test. All sample surface's BACs shifted towards a middle value; the rougher specimens were smoothed and the smoother specimens were roughened.

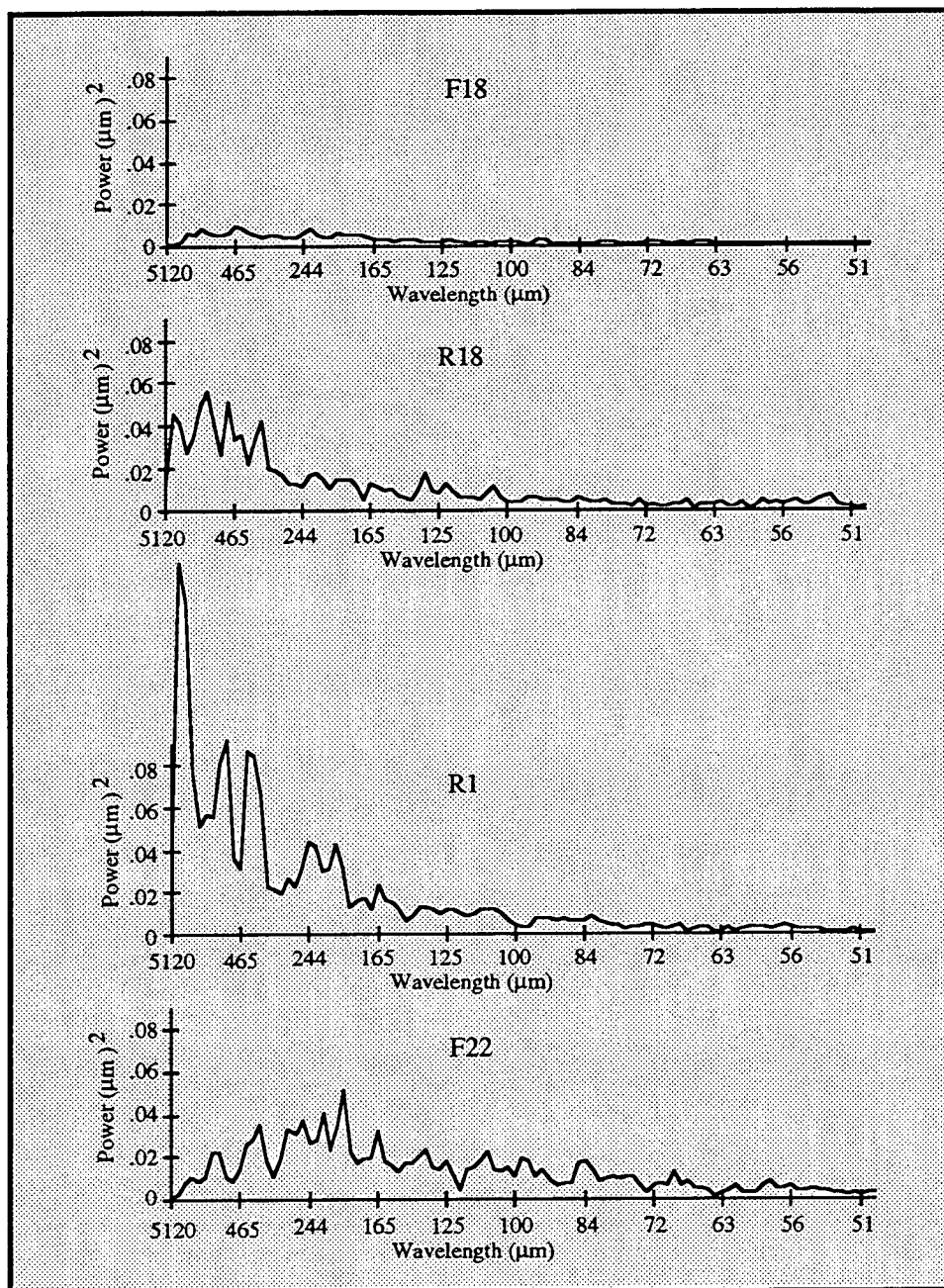
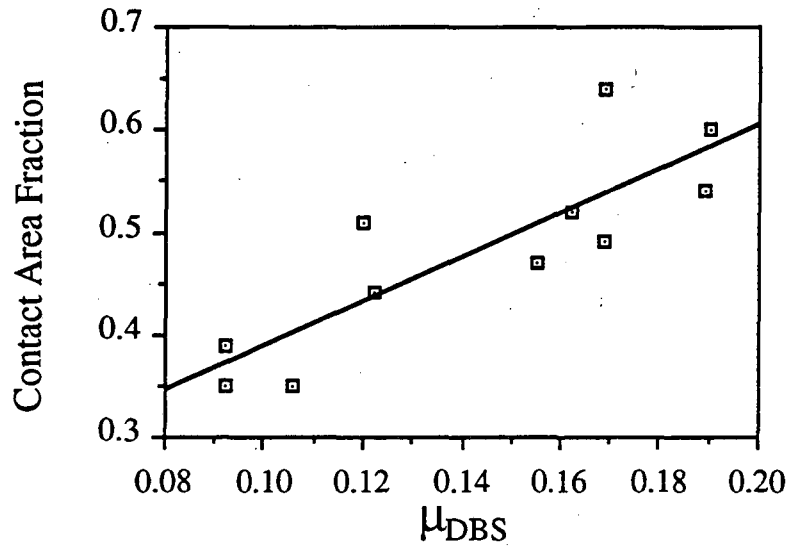


Figure 6: Power spectra of four commercial samples, F18 and R18 exhibit low friction in the DBS test, R1 and F22 exhibit high friction. Higher roughness (more area under the spectrum) corresponds to lower friction (F22, R1). If the roughness is distributed to shorter wavelengths, as with F22, the overall roughness does not need to be as great to produce low friction. R18 has the same roughness as F22, but since it is concentrated in the longer wavelengths, it is not as effective.

a) Commercial Samples



b) Laboratory Coated Samples

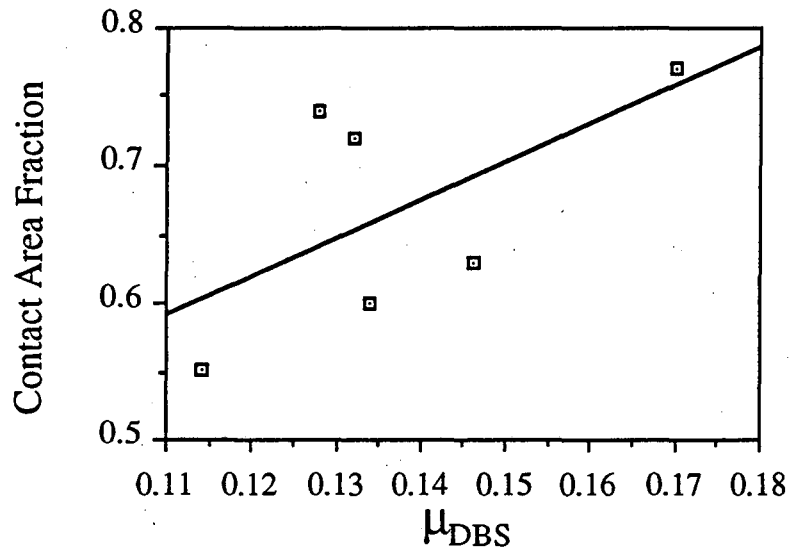


Figure 7: Area fraction deformed as a function of coefficient of friction in the Drawbead Simulator test, μ_{DBS} .

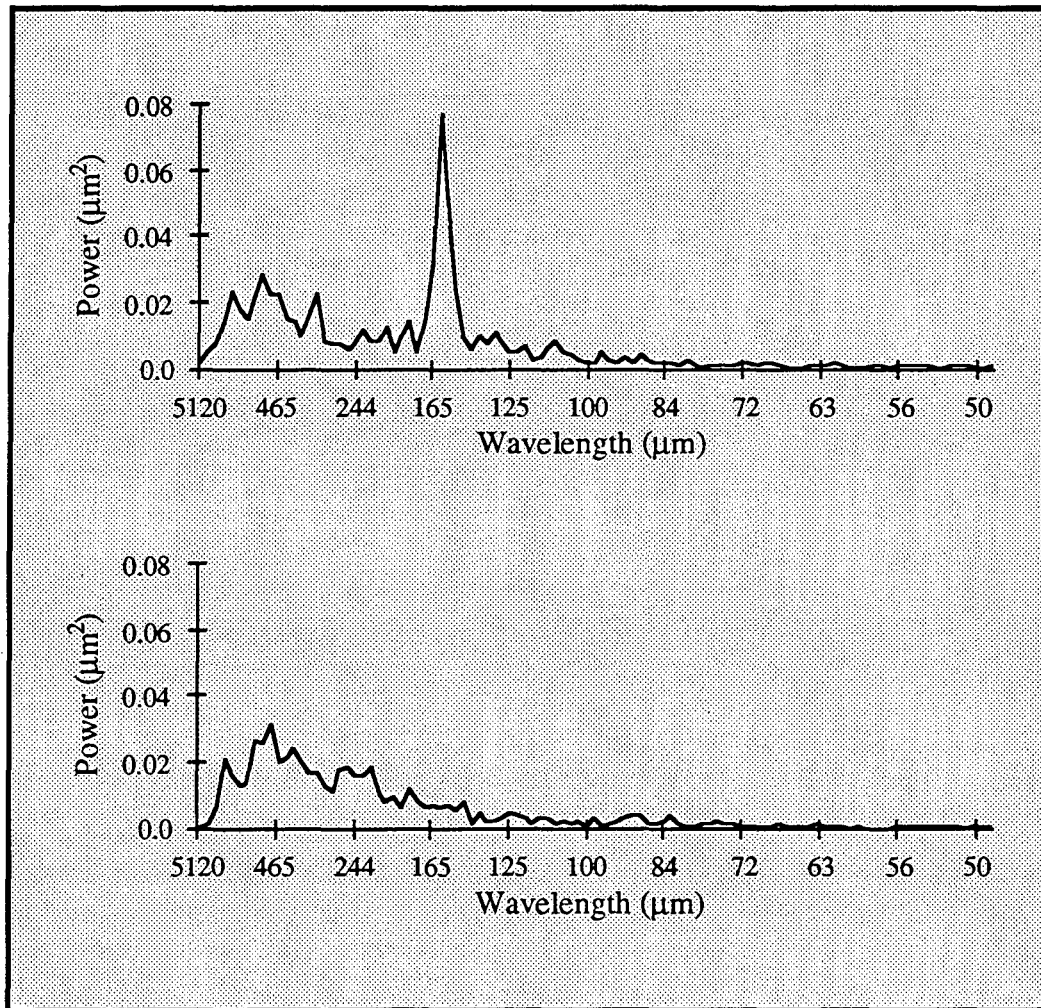


Figure 8: Longitudinal and transverse power spectra from a lasertex sample.

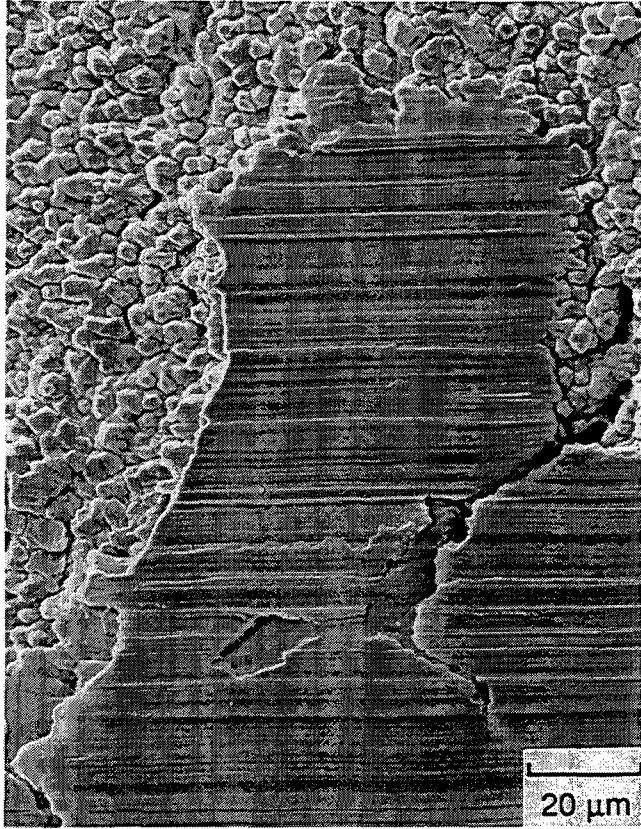
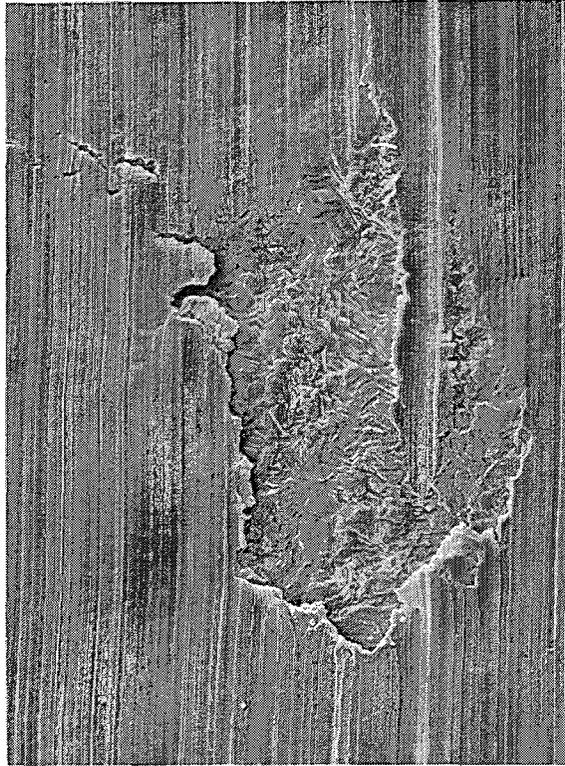


Figure 9: Deformed surface showing the persistence of the micro-roughness in valleys



20 μm

Figure 10: Deformed surface showing region where the lubricant was trapped.

REFERENCES

- 1 Fontana, M.G., Greene, N.D., **Corrosion Engineering**, McGraw Hill, New York, 1978, pp 266-267.
- 2 Barrett, C., Nix, W., Tetelman, A., **The Principles of Engineering Materials**, Prentice-Hall, Inc., Englewood Cliffs, New Jersey, 1973, pp 185-187.
- 3 Shaffer, S.J., **Micromechanisms of Friction in Electrogalvanized Sheet Steel with Emphasis on the Role of Texture**, PhD. Thesis, 1990, p. 1.
- 4 Izvorski, N., Personal Communication, Ford Motor Company Data, April, 1988.
- 5 Adamson, A., **Physical Chemistry of Surfaces**, John Wiley and Sons, 1990, pp. 460-488.
- 6 Amonton, G., **De la resistance causee dans les machines**, *Memoires de l'Academie Royale A*, 1699, pp. 275-282.
- 7 Bowden, P. and Tabor, E., **The Friction and Lubrication of Solids**, Oxford University Press, 1964.
- 8 Rabinowicz, E., **Friction and Wear of Materials**, John Wiley and Sons, 1965.
- 9 Schey, J.A., **Tribology in Metalworking: Friction, Lubrication and Wear**, ASM, 1983.
- 10 Campbell, W. E., **Boundary Lubrication**, *Boundary Lubrication, An Appraisal of World Literature*, ASME, 1969, pp. 87-118.
- 11 Komvopoulos, K. et al., **The Mechanism of Friction in Boundary Lubrication**, *Journal of Tribology*, Vol. 107, pp. 452-462.
- 12 Komvopoulos, K., Saka, N., and Suh, N.P., **Plowing Friction in Dry and Lubricated Metal Sliding**, *Journal of Tribology*, Vol. 108, 1986.
- 13 Suh, N.P. and Sin, H.-C., **The Genesis of Friction**, *Wear*, Vol. 69, 1981, pp. 91-114.
- 14 Buckley, D.H., and Johnson, R.L., **The Influence of Crystal Structure and Some Properties of Hexagonal Metals on Friction and Adhesion**, *Wear*, v.2, 1968, pp. 405-419.
- 15 Buckley, D.H., **Influence of Crystal Orientation on Frictional Characteristics of Titanium Single Crystals in Vacuum**, NASA TN D-2988, 1965.
- 16 Rangarajan, V., Matlock, D.K., and Krauss, G., **Effects of Coating Properties on the Friction Response of Zinc Coated Sheet Steels**, *Zinc-Based Steel Coating Systems: Metallurgy and Performance*, G. Krauss & D. K. Matlock, eds., TMS, Warrendale, PA, 1990, pp. 263-280.

- 17 Lindsay, J.H., Paluch, R.F., Nine, H.D., Miller, V.R., and O'Keefe, T.J., **The Interaction Between Electrogalvanized Zinc Deposit Structure and the Forming Properties of Sheet Steel**, *Plat. and Surf. Finishing*, v.76, 1989, no.3, pp. 62-69.
- 18 Shaffer, S.J., Nojima, W.E., Skarpelos, P.N., and Morris, J.W. Jr., **Research on the Metallurgical Determinants of Formability in Electrogalvanized Sheet**, *Zinc-Based Steel Coating Systems: Metallurgy and Performance*, G. Krauss & D. K. Matlock, eds., TMS, Warrendale, PA, 1990, pp. 251-262.
- 19 Nakamori, T. and Shibuya, A., **Effects of Galvannealing Conditions and Coating Weight on Powdering Resistance of Galvannealed Steel Sheet**, *Corrosion Resistant Automotive Sheet Steel*, ed. L. Allegra, ASM, Metals Park, OH, 1988, pp. 139-149.
- 20 Hisamatsu, Y., **Science and Technology of Zinc and Zinc Alloy Coated Steel Sheet**, *Proc. GALVATECH '89, International Conference of Zinc and Zinc Alloy Coated Steel Sheet*, September 5-7, Tokyo, ISIJ, 1989, pp. 3-12.
- 21 Pak, S.-W., and Meshii, M., **Structure-Mechanical Property Relation in Zinc Electrogalvanized Coatings**, *Zinc-Based Steel Coating Systems: Metallurgy and Performance*, G. Krauss & D. K. Matlock, eds., TMS, Warrendale, PA, 1990, pp. 357-369.
- 22 Rangarajan, V., Giallonrakis, N.M., Matlock, D.K., and Krauss, G., **The Effect of Texture and Microstructure on Deformation of Zinc Coatings**, *Journal of Materials Shaping Technology*, v.6, no.4, (1989), pp. 217-227.
- 23 Nakamura, S., Yoshida, M., Nishimoto, A. **Frictional Characteristics of Coated Steel Sheets**, *Proceedings of the 15th Biennial Congress of the IDDRG*, ASM International, 1988, pp. 77-84.
- 24 Hilson, R., Bernick, R., **Development of a Quantitative Sheet Galling Test**, *Wear*, June 1978, v.48, no.2, pp 323-346.
- 25 Marique C., Bonnarens H., Richelmi J., Bragard A., **Caracterisation de la Morphologie de Surface des Toles Mince Laminees a Froid**, Final report ECSC/CRM agreement 6210/kc2-203, 1979.
- 26 Schedin, E., Fredriksson, K., Gustafsson, C., **Characterization of Friction Properties During Sheet Forming**, *Proceedings of the 15th Biennial Congress of the IDDRG*, ASM International, 1988, pp.55-62.
- 27 Bragard, A. et al. **Present State of CRM Work Related to Surface Analysis of Cold Rolled Steel Sheets**, *Proceedings of the 10th IDDRG Congress*, Warcorek, ASM International, 1978, p 259.
- 28 Emmens, W. C. and Hartman L., **The Effect of Surface Roughness on the Formability of Cold Reduced Sheet Steel**, *Proceedings of the 13th IDDRG Congress*, Melbourne Australia, ASM International, 1984.

- 29 Emmens, W.C., **The Influence of Surface Roughness on Friction**, *Proceedings of the 15th Biennial Congress of the IDDRG*, ASM International, 1988, pp.63-70.
- 30 Montfort, G., Defourny J. and Bragard A., **Progress in the Roughness Texture of the Cold Rolled Steel Sheets Related to Deep Drawing and Forming**, *Proceedings of the 15th IDDRG Congress*, Dearborn Michigan, ASM International, 1988.
- 31 Rault, D., Etringer, M., **Antigalling Roughness Profile Permitting the Reduction of Blank Holder Pressure and the Required Amount of Lubricant During the Forming of the Sheet**, *Proceedings of the 9th IDDRG Congress*, Ann Arbor Michigan , ASM International, 1976, p 97.
- 32 Christensen, H., **Some Aspects of the Functional Influence of Surface Roughness in Lubrication**, *Wear*, 17, 1971, pp. 149-162.
- 33 Littlewood, M., **The Effect of Surface finish and Lubrication on the Frictional Variations Involved in the Sheet Metal Forming Process**, *Proceedings of the BDDRG Colloquium on Fundamental Considerations in Sheet Metal Forming*, 1964.
- 34 Wilson, W.R.D., **Friction and Lubrication In Sheet Metal Forming**, *Proceedings of an International Symposium on Mechanics of Sheet Metal Forming*, Plenum Press, 1978, pp.157-174.
- 35 Bragard A., et al., **La Surface des Toles d'Acier Dans Les Problemes d'Emboutissage**, Convention ECSC/CRM 7210-KD/205, 1983, publ. EUR. Luxembourg.
- 36 Nine H.D., **Drawbead Forces in Sheet Metal Forming**, *Proceedings of an International Symposium on Mechanics of Sheet Metal Forming*, Plenum Press, 1978, pp.179-207.
- 37 H.D. Nine, **The Applicability of Coulomb's Friction Law to Drawbeads in Sheet Metal Forming**, *J. of Applied Metalworking*, v.2 no.3, July 1982, pp 200-210.
- 38 Wang, N.M., **A Mathematical Model of Drawbead Forces in Sheet Metal Forming**, *J. Applied Metalworking*, v 2, no.3, July 1982, pp 193-199.
- 39 Stoughton, T.B., **Model of Drawbead Forces in Sheet Metal Forming**, *Proceedings of an International Symposium on Mechanics of Sheet Metal Forming*, Plenum Press, 1978, pp.205-215.
- 40 American National Standard Institute, **Surface Texture (Surface Roughness, Waviness, and Lay)**, ANSI/ASME B46.1, 1985.
- 41 Thomas, T.R., **Rough Surfaces**, Longman Inc., New York, 1982.
- 42 Dagnall, H., **Exploring Surface Texture**, Rank Taylor Hobson Ltd., Leicester, England, 1986.

- 43 Whitehouse, D.J., **Modern Methods of Assessing the Quality and Function of Surface Texture**, RTH (Reprinted from Modern Workshop Technology, Part 2, Macmillan and Co, Ltd.) 1970.
- 44 Press, W.H., Flannery, B.P., Teukolsky, S.A., Vetterling, W.T., **Numerical Recipes, The Art of Scientific Computing**, Cambridge University Press, Cambridge MA, 1989.
- 45 Champeney, D.C., **Fourier Transforms and Their Physical Applications**, Academic Press, New York NY, 1973.
- 46 Brigham, E. O., **The Fast Fourier Transform**, Prentice-Hall, Englewood NJ, 1974.
- 47 Elliot, D.F., and Rao, K.R., **Fast Transforms: Algorithms, Analyses, Applications**, Academic Press, New York NY, 1982.
- 48 Muller, R., **Evaluation of the Properties of Sheet With Lasertex Surface Texture**, Proceedings of the 15th IDDRG Congress, Dearborn Michigan, ASM International, 1988.
- 49 Aku, P. M., Ed., **Interdisciplinary approach to Friction and Wear**, *Proceedings of a Nasa-sponsored symposium*, U.S. Government Printing Office, 1967.
- 50 Challen, J.M. and Oxley, P.L., **An Explanation of the Different Regimes of Friction and Wear Using Asperity Deformation Models**, *Wear*, v.53, 1979, pp 229-243.
- 51 Komvopoulos, K., **Fundamentals of Tribology and Contact Mechanics**, U.C. Berkeley, 1990.
- 52 Green, A.P., **The Plastic yielding of Metal Junctions due to Combined Shear and Pressure**, *Journal of the Mechanics and Physics of Solids*, v. 2, 1954, pp 197-211.
- 53 Challen, J.M., and Oxley, P.L.B., **An Explanation of the Different Regimes of Friction and Wear Using Asperity Deformation Models**, *Wear*, v. 53, 1979, pp 229-243.
- 54 Komvopoulos, K., Saka, N., Suh, N.P., **Plowing Friction in Dry and Lubricated Metal Sliding**, *Journal of Tribology*, v. 108, 1986, pp 301-313.
- 55 Wanheim, T., and Bay, N., **A Model for Friction in Metal Forming Processes**, *CIRP Annals: Manufacturing Technology*, 1978, pp. 189-194.
- 56 Nojima, W., **Effect of Lubricant Additives and Viscosity on Formability of Galvanized Steel Sheet**, M.S. Thesis, U.C. Berkeley, 1992.
- 57 Schey, J.A., and Dalton, G.M., **Lubrication Mechanisms in the Forming of Galvanized Steel Sheet**, *Journal of Materials Processing Technology*, v. 24, 1990, 365-374.

APPENDIX A: POWER SPECTRA

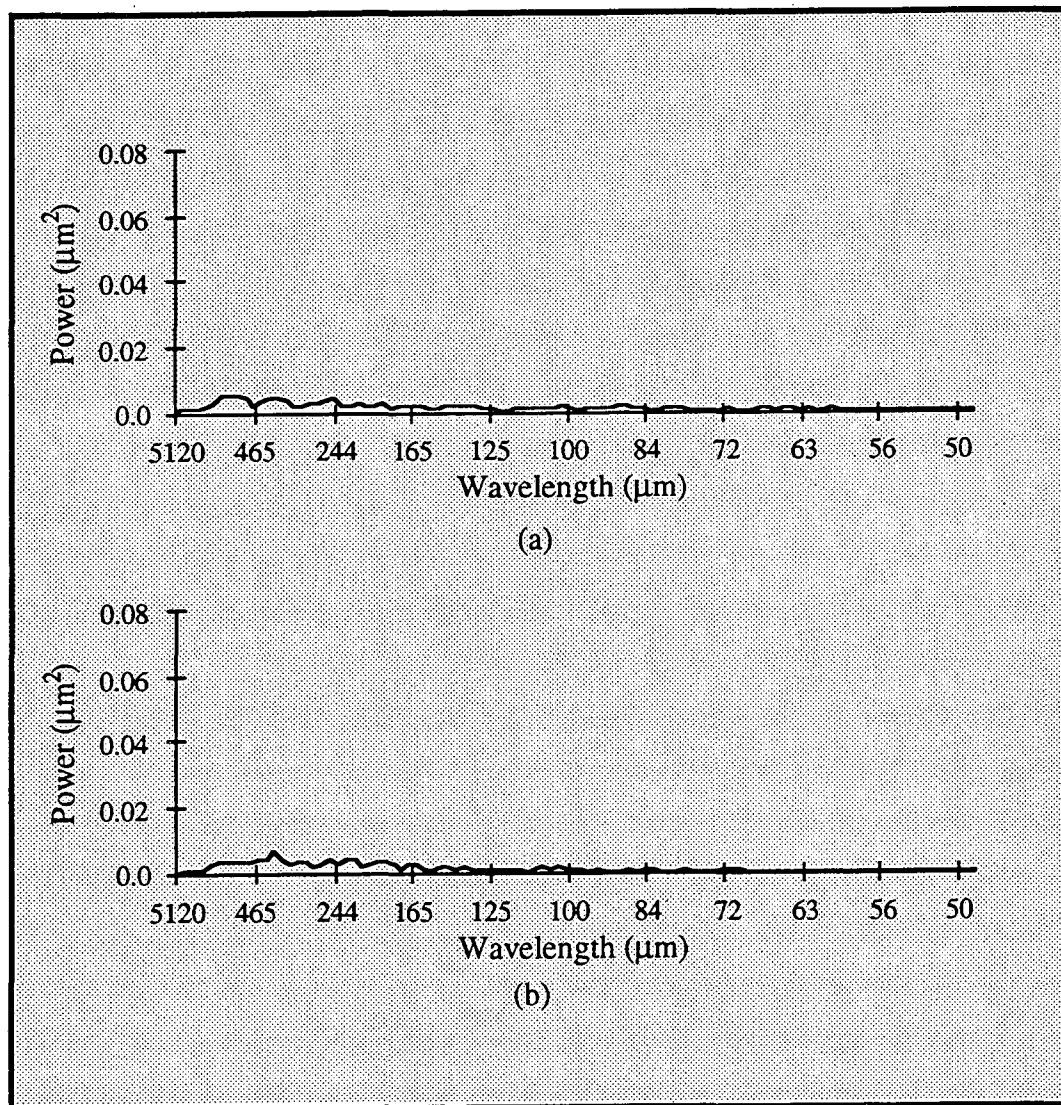


Figure A1: Power Spectra from commercial specimen F14: (a) traces in rolling direction; (b) traces in transverse direction.

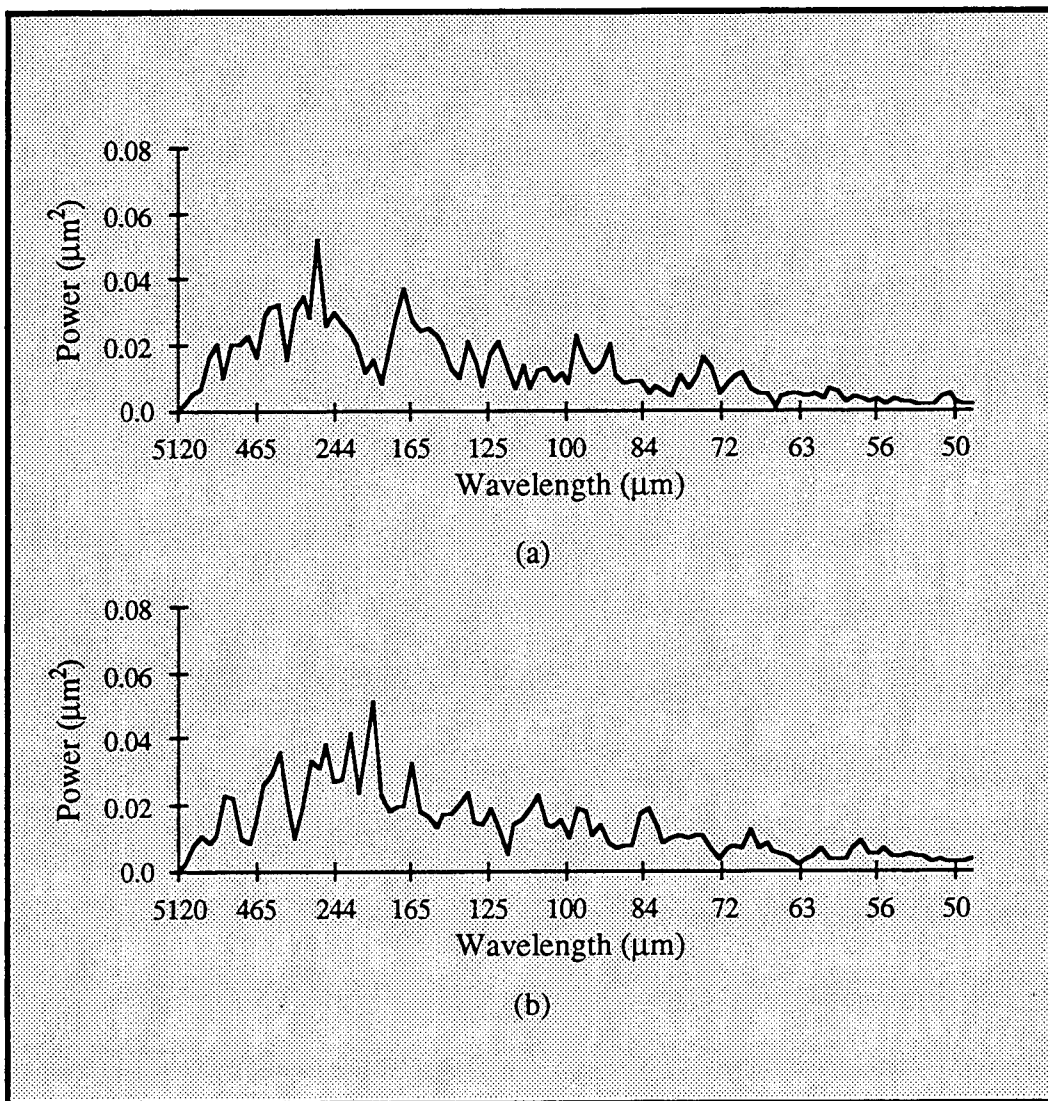


Figure A2: Power Spectra from commercial specimen F22 (a) traces in rolling direction; (b) traces in transverse direction.

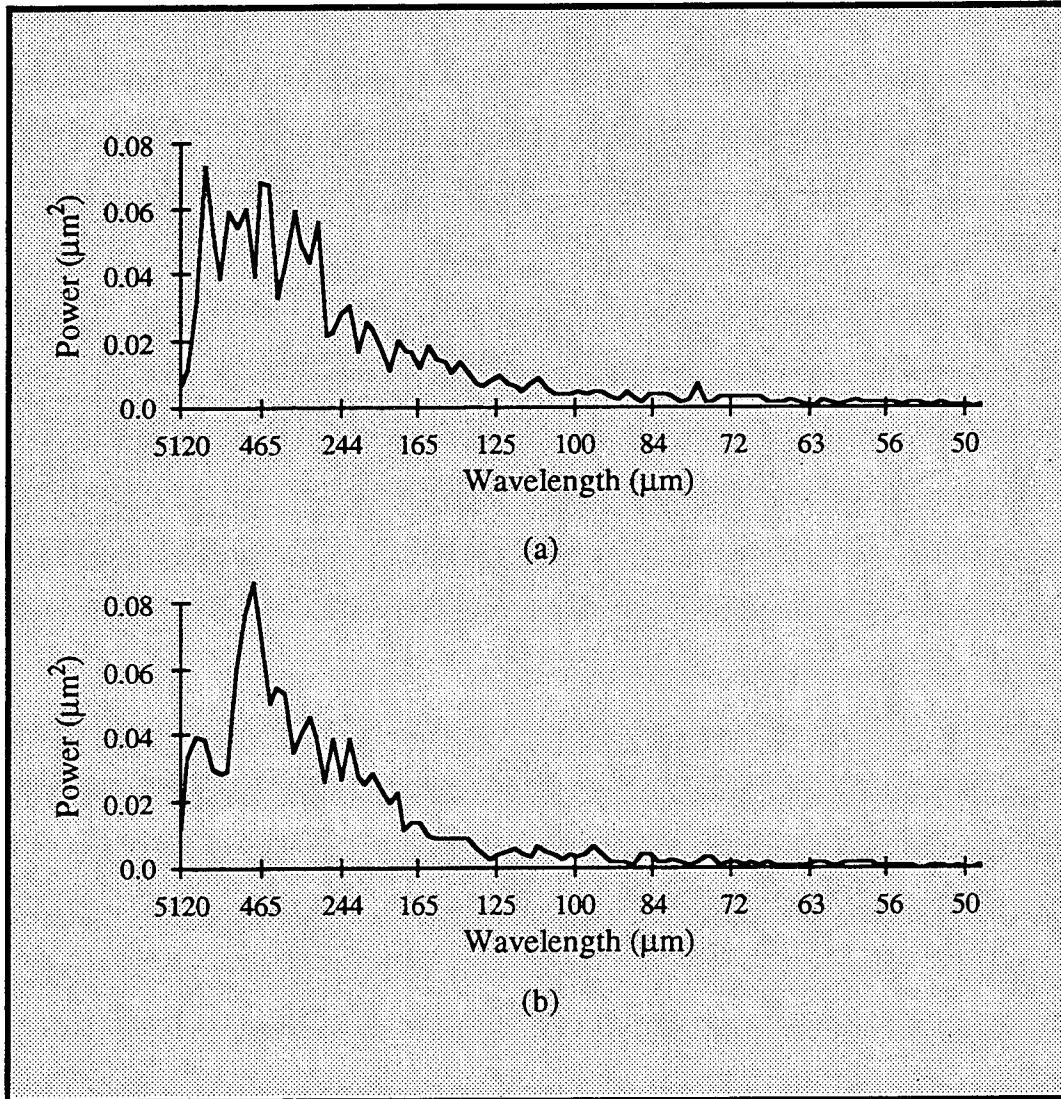


Figure A3: Power Spectra from commercial specimen RLO (a) traces in rolling direction; (b) traces in transverse direction.

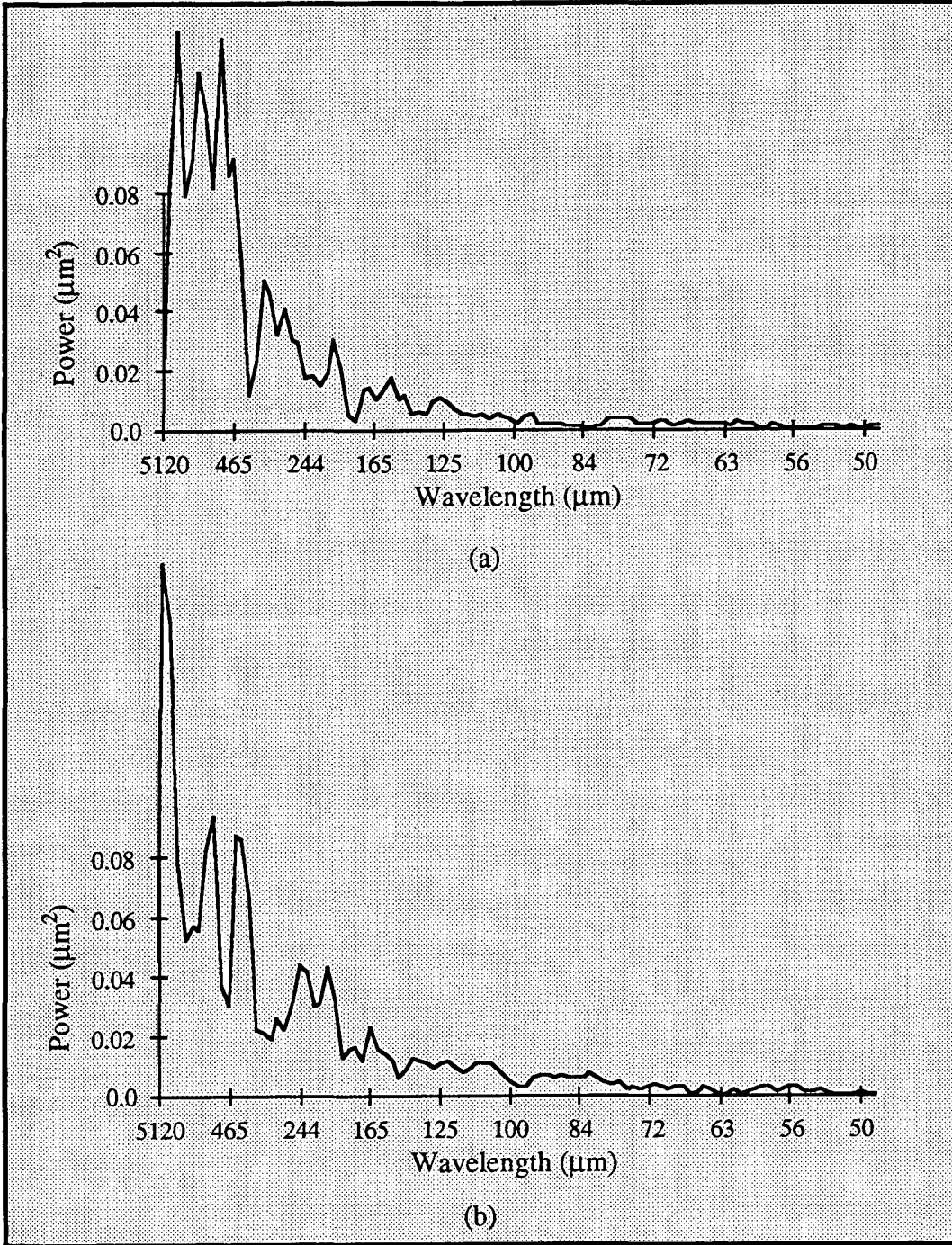


Figure A4: Power Spectra from commercial specimen **R1** (a) traces in rolling direction; (b) traces in transverse direction.

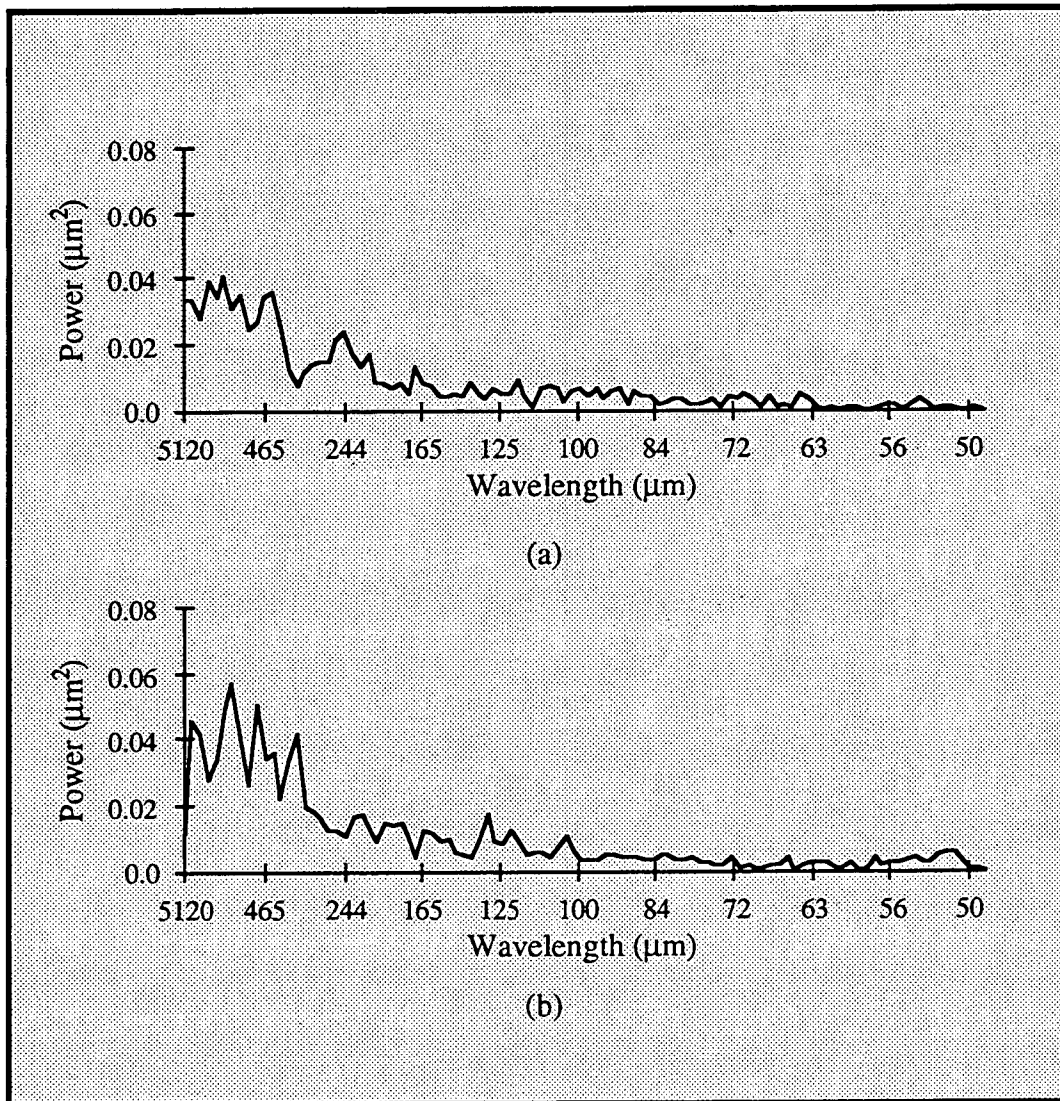


Figure A5: Power Spectra from commercial specimen R18 (a) traces in rolling direction; (b) traces in transverse direction.

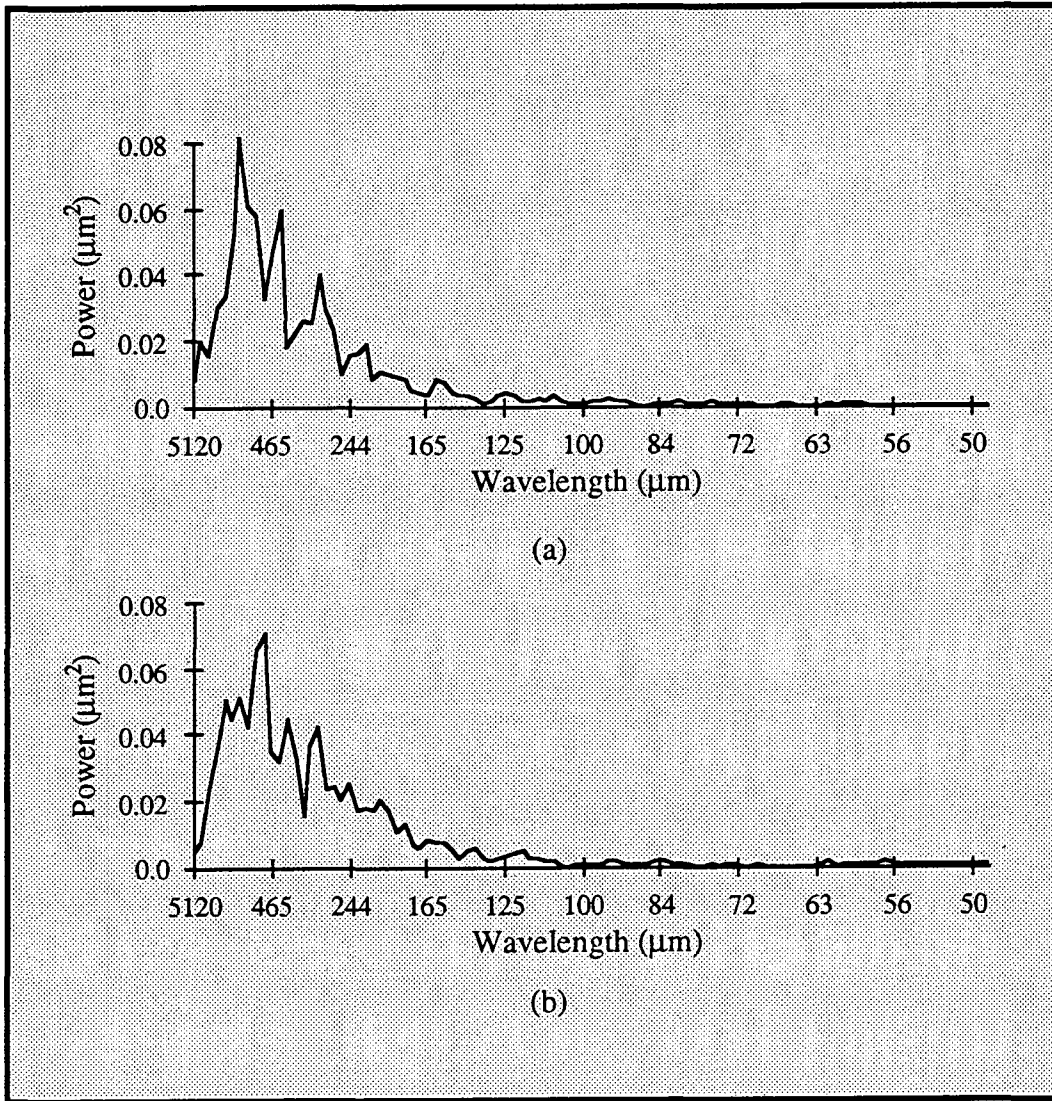


Figure A6: Power Spectra from commercial specimen R3706 (a) traces in rolling direction; (b) traces in transverse direction.

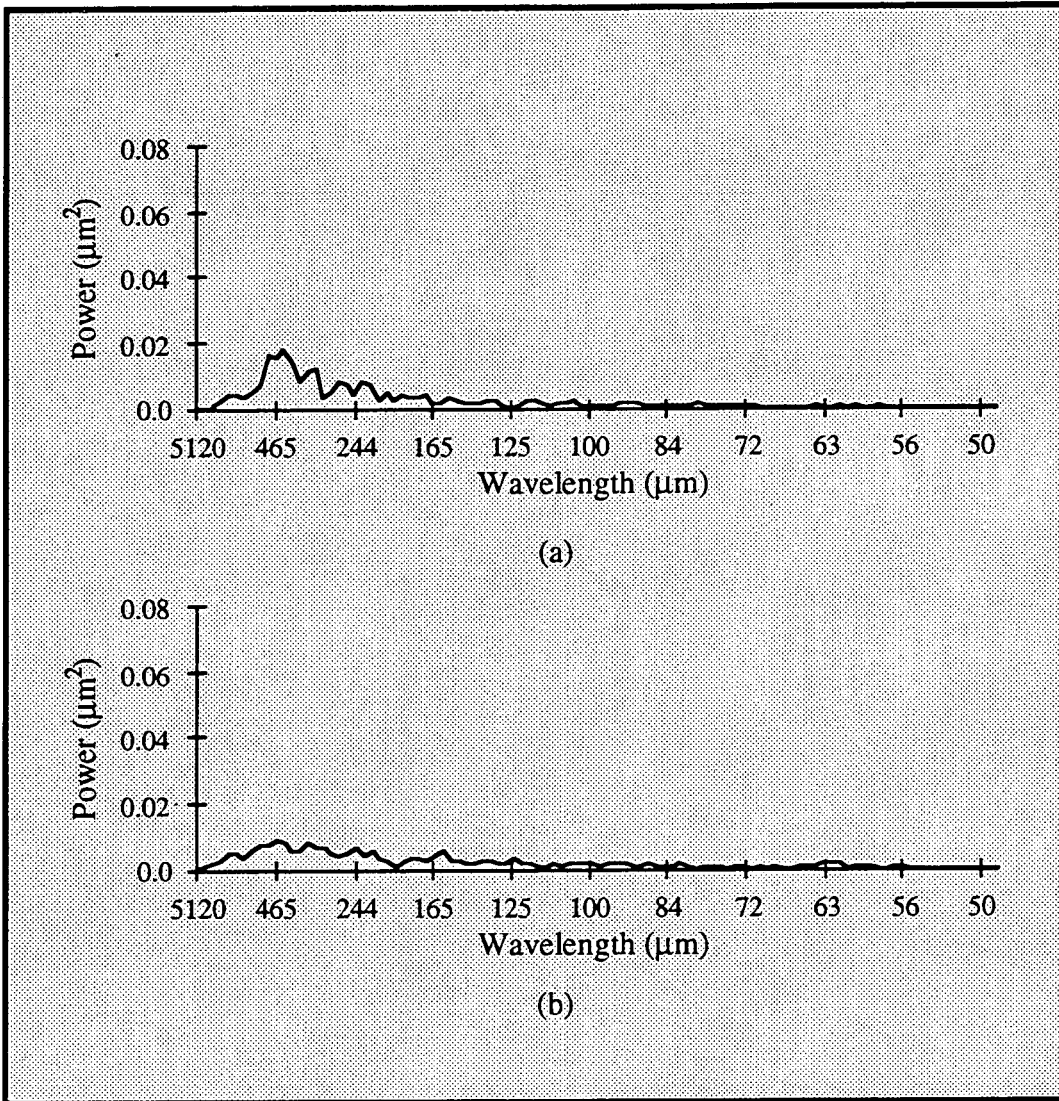


Figure A7: Power Spectra from commercial specimen USX (a) traces in rolling direction; (b) traces in transverse direction.

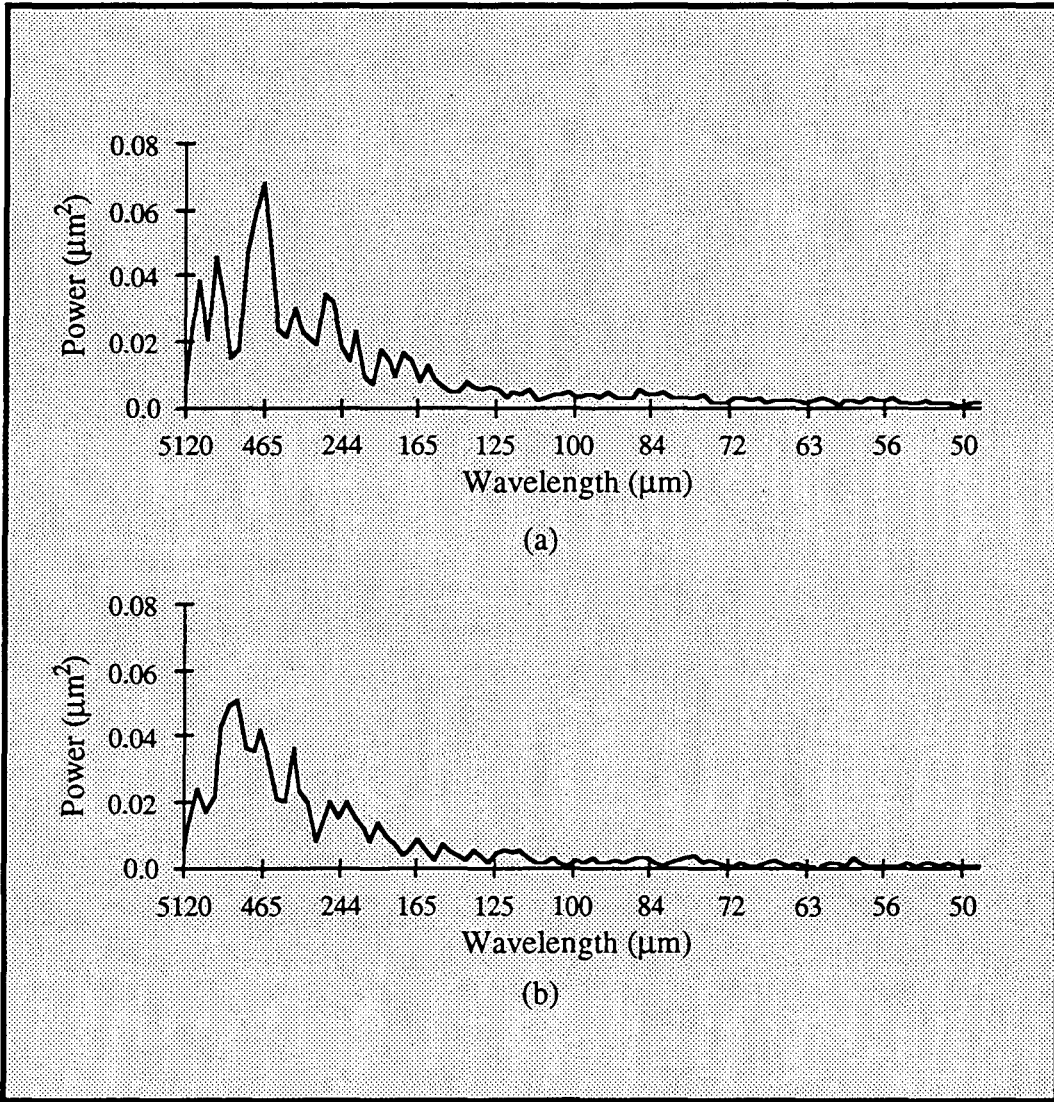


Figure A8: Power Spectra from commercial specimen **F5** (a) traces in rolling direction; (b) traces in transverse direction.

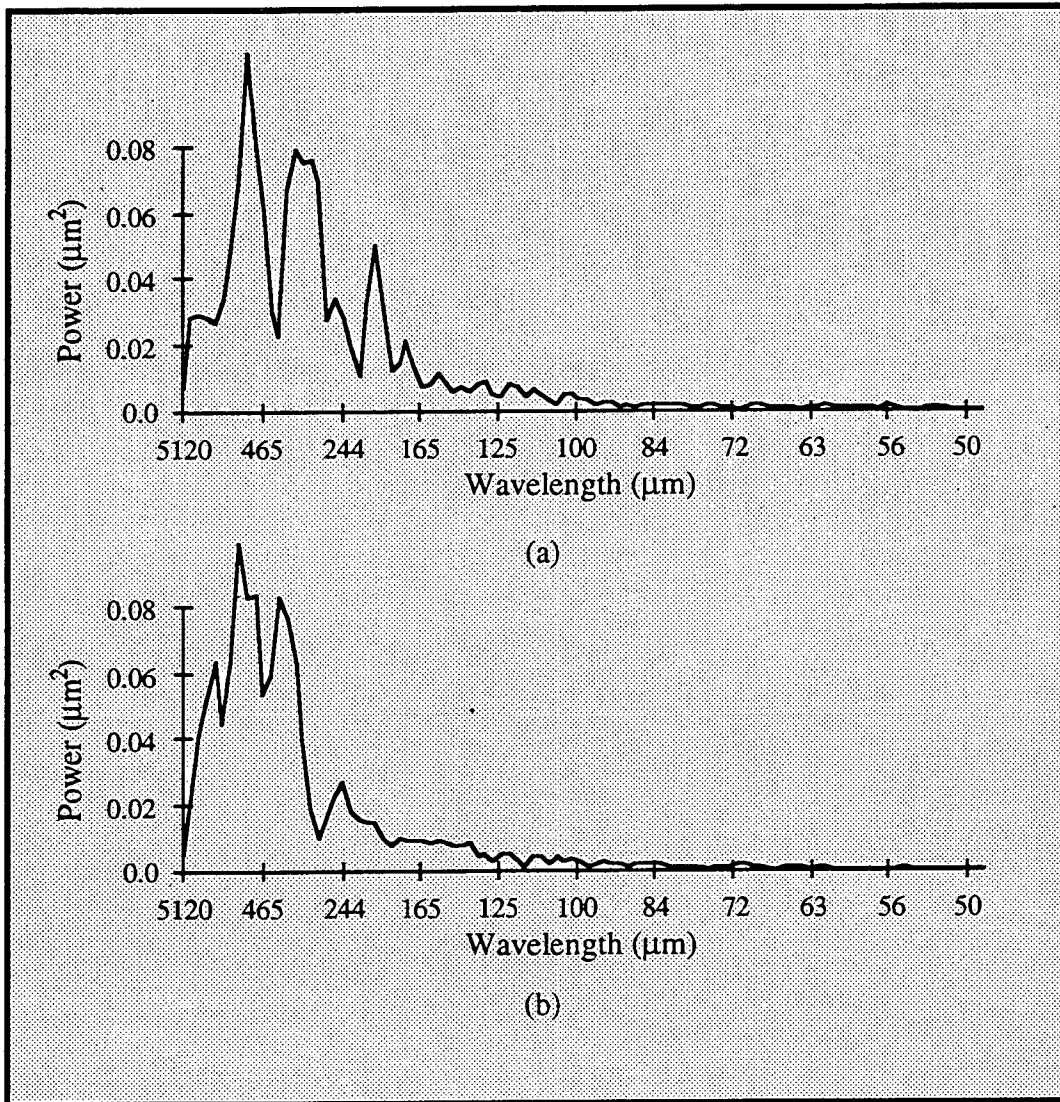


Figure A9: Power Spectra from commercial specimen **RC** (a) traces in rolling direction; (b) traces in transverse direction.

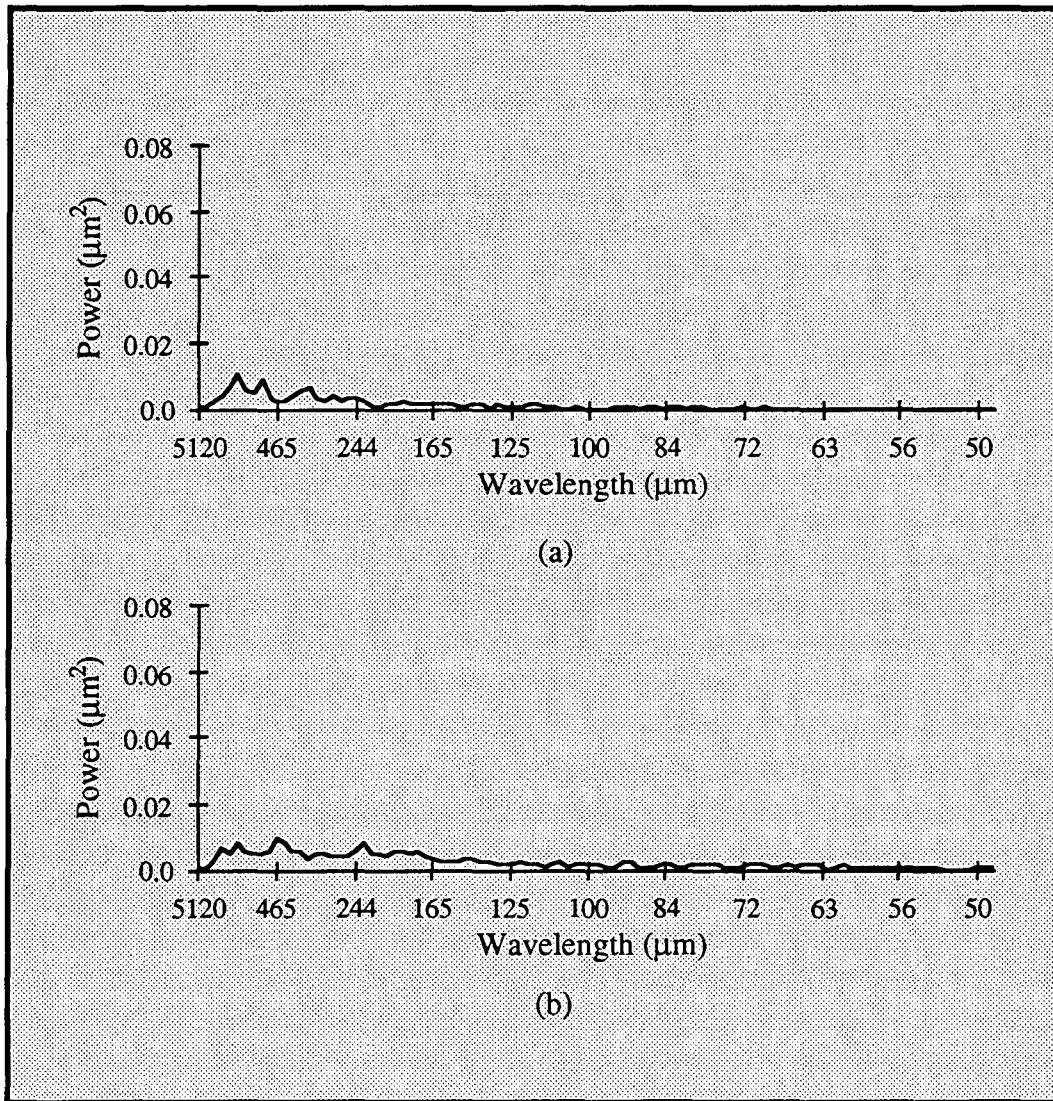


Figure A10: Power Spectra from commercial specimen F18 (a) traces in rolling direction; (b) traces in transverse direction.

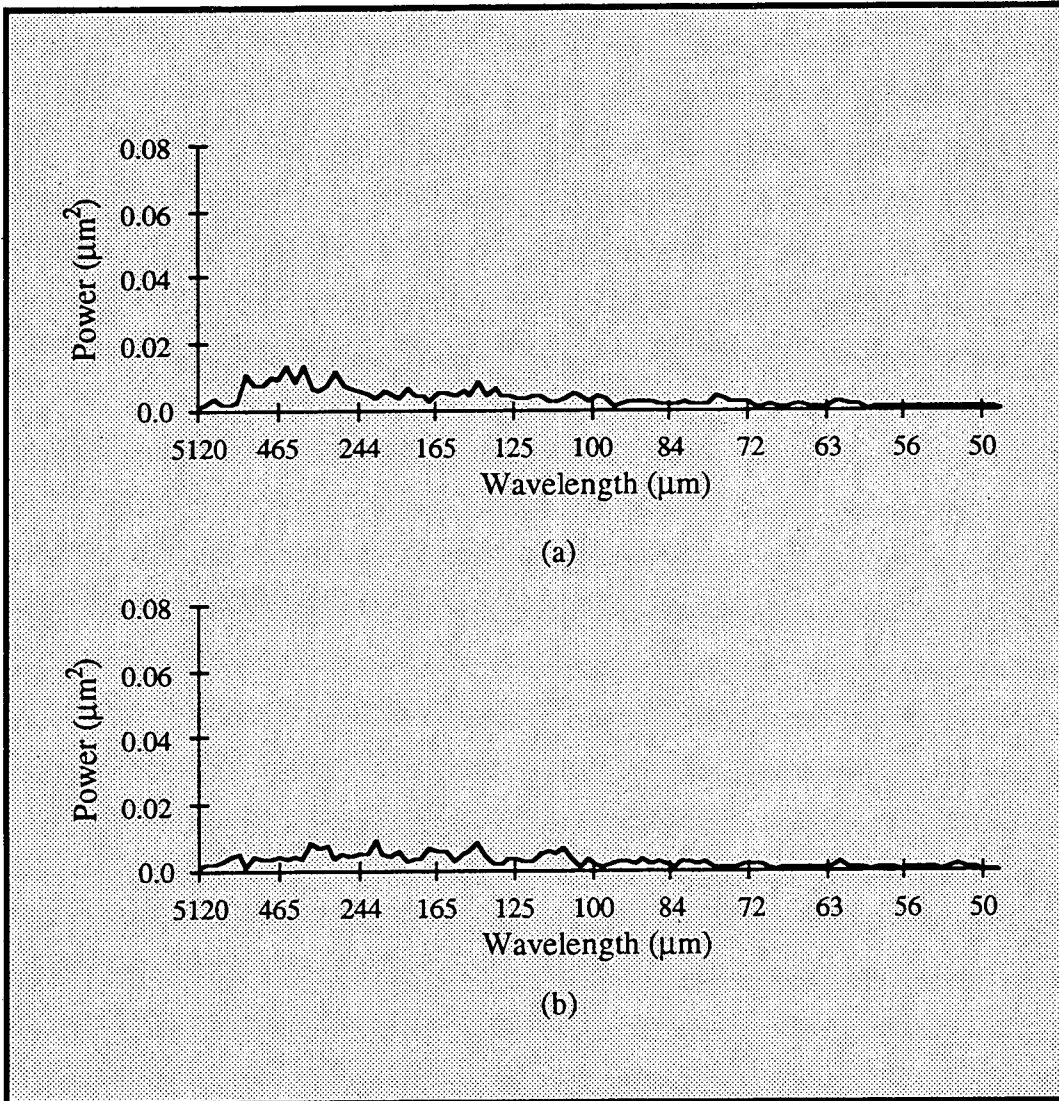


Figure A11: Power Spectra from commercial specimen **VR410** (a) traces in rolling direction; (b) traces in transverse direction.

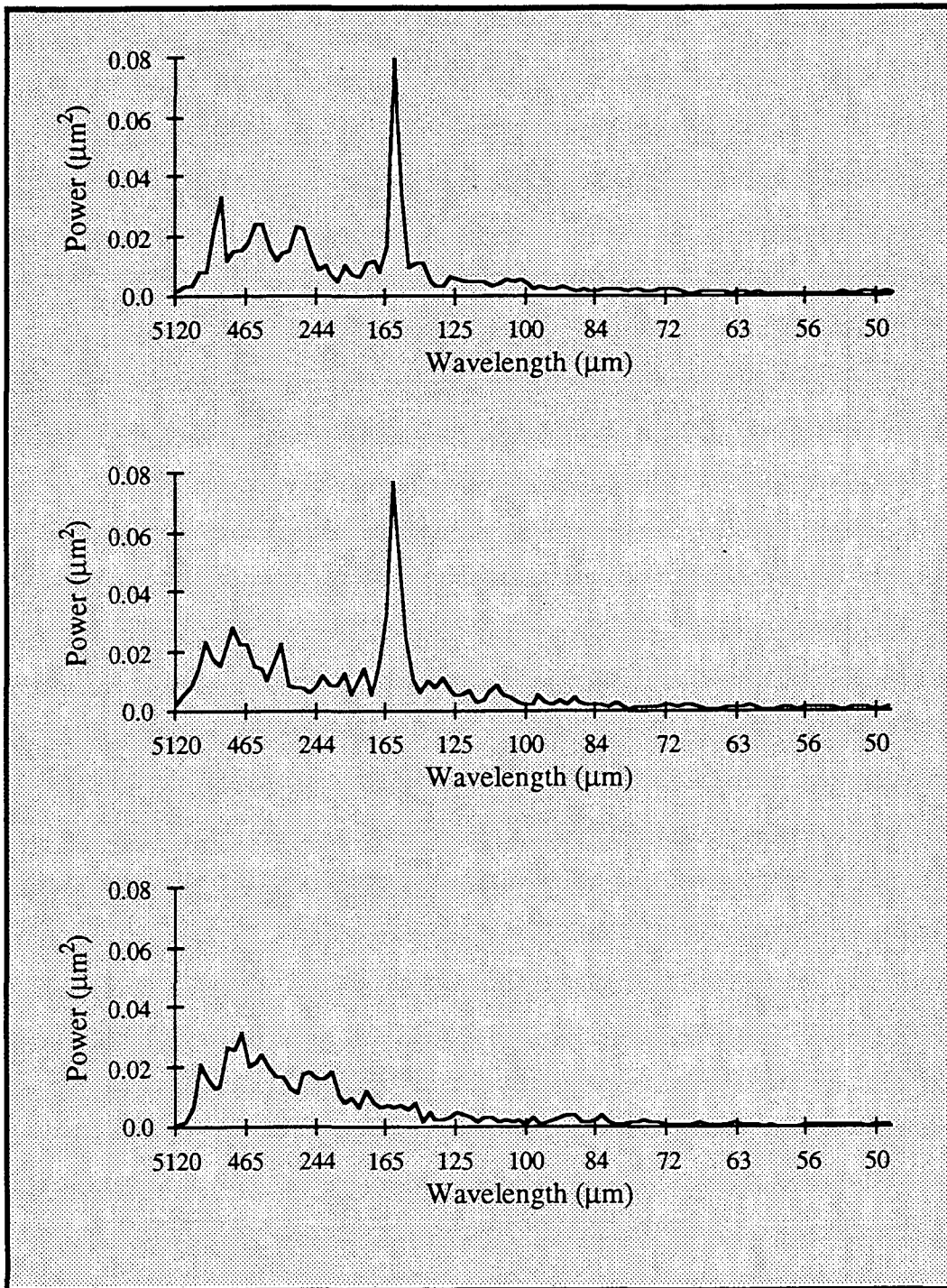


Figure A12: Power Spectra from laboratory coated specimen **Laser 1:**
 (a) uncoated, traces in rolling direction; (b) coated, traces in rolling
 direction; (c) coated, traces in transverse direction.

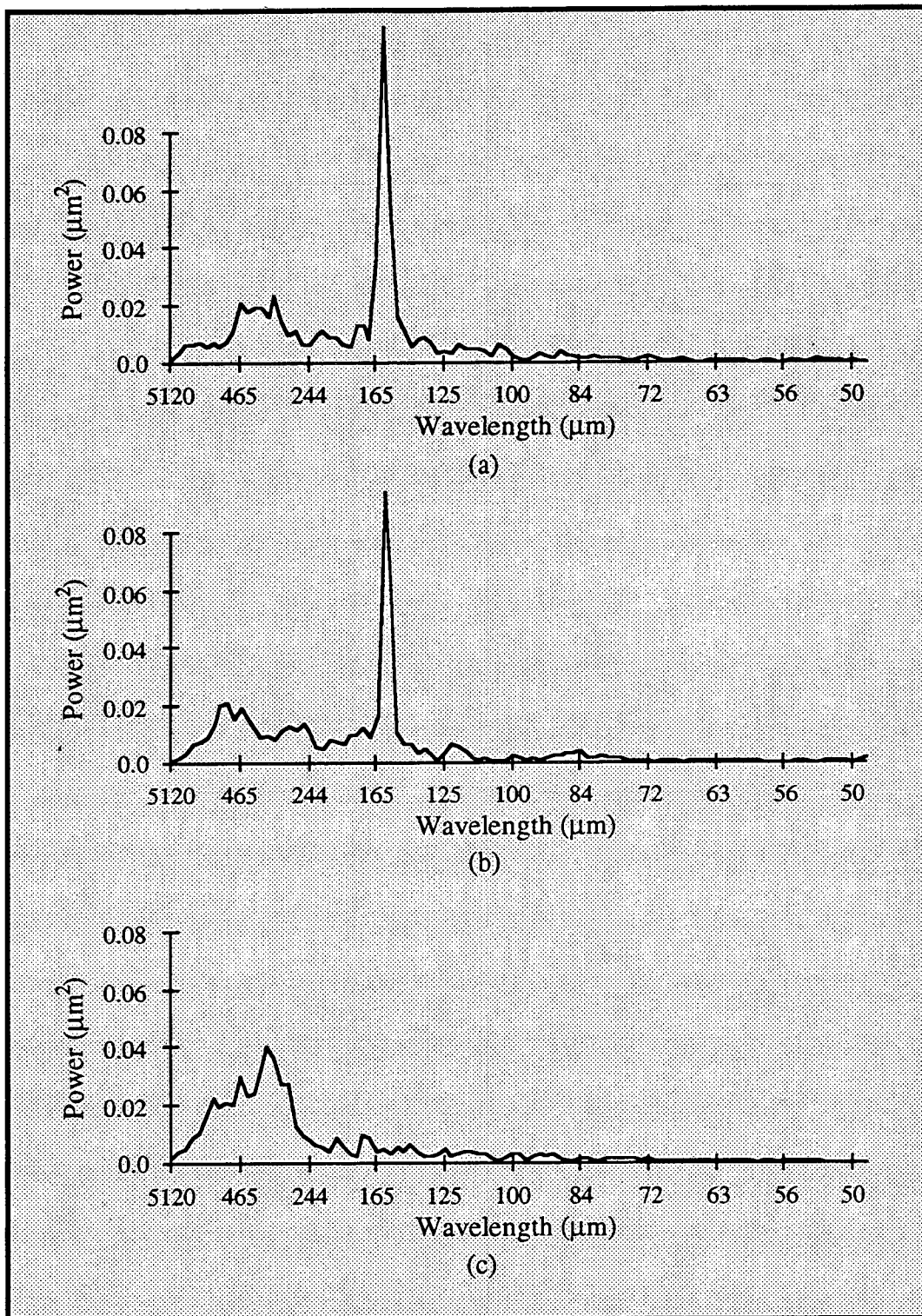


Figure A13: Power Spectra from laboratory coated specimen **Laser 2**: (a) uncoated, traces in rolling direction; (b) coated, traces in rolling direction; (c) coated, traces in transverse direction.

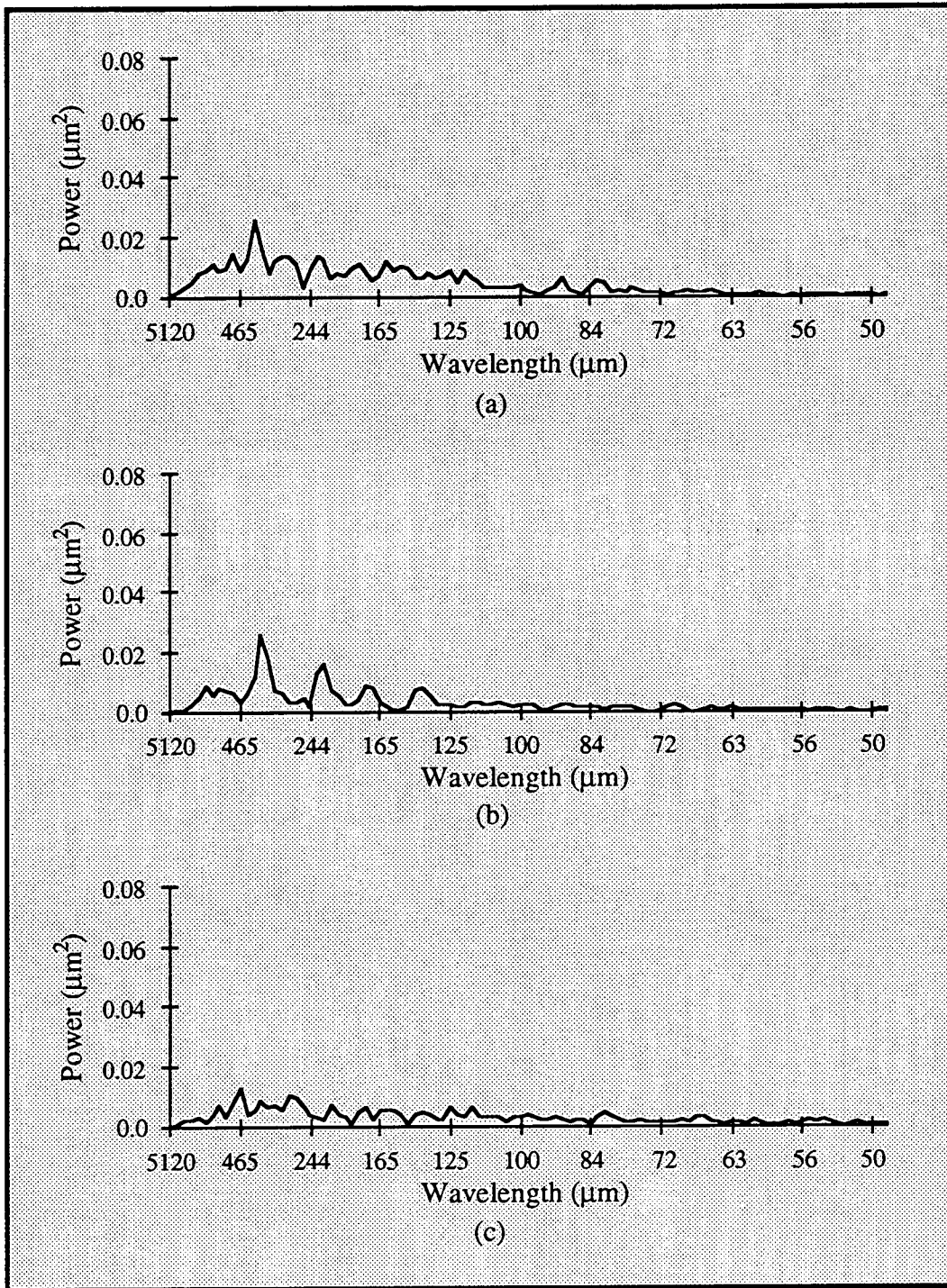


Figure A14: Power Spectra from laboratory coated specimen **Shot Blast 1:** (a) uncoated, traces in rolling direction; (b) coated, traces in rolling direction; (c) coated, traces in transverse direction.

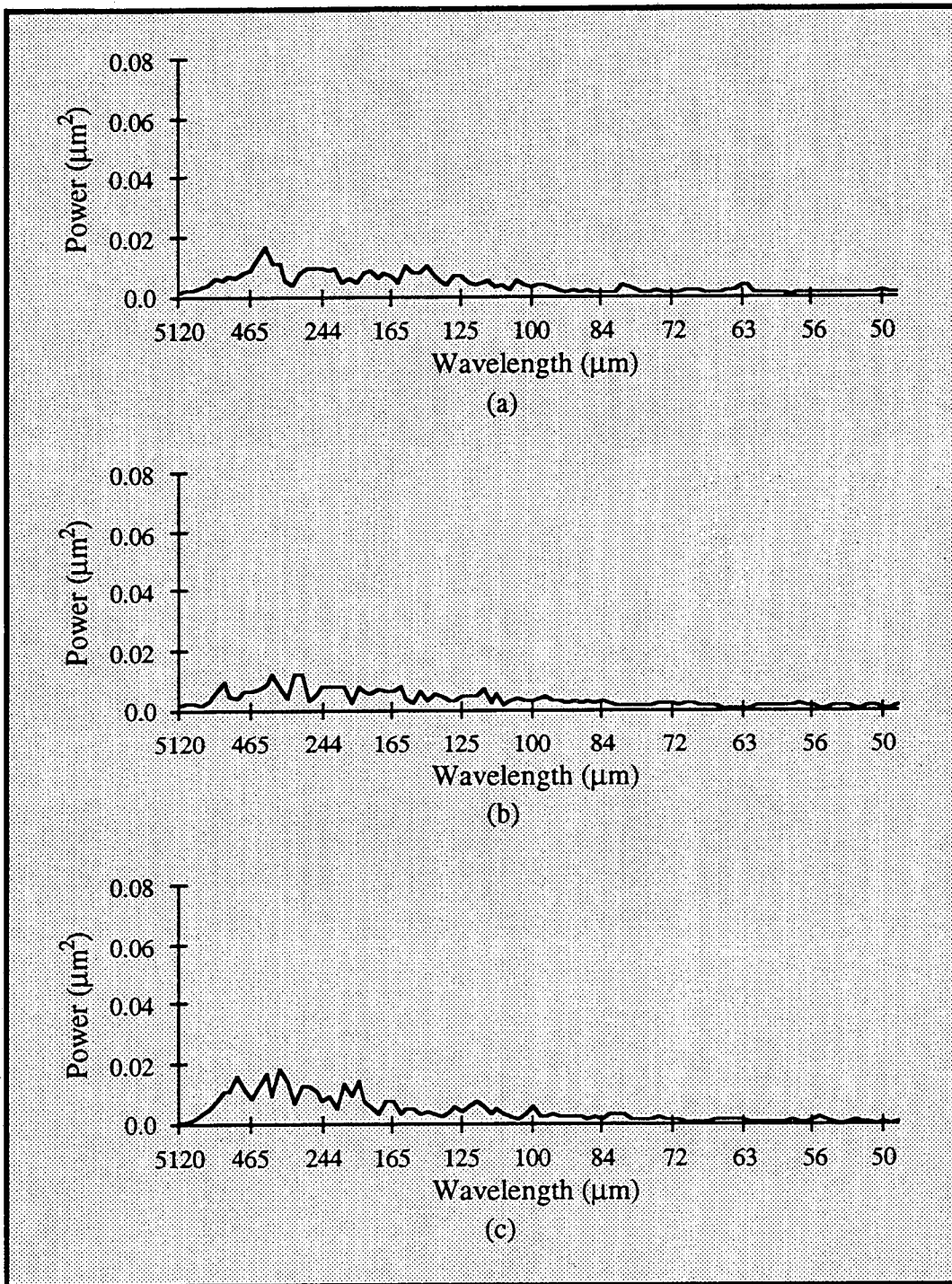


Figure A15: Power Spectra from laboratory coated specimen Shot Blast 2: (a) uncoated, traces in rolling direction; (b) coated, traces in rolling direction; (c) coated, traces in transverse direction.

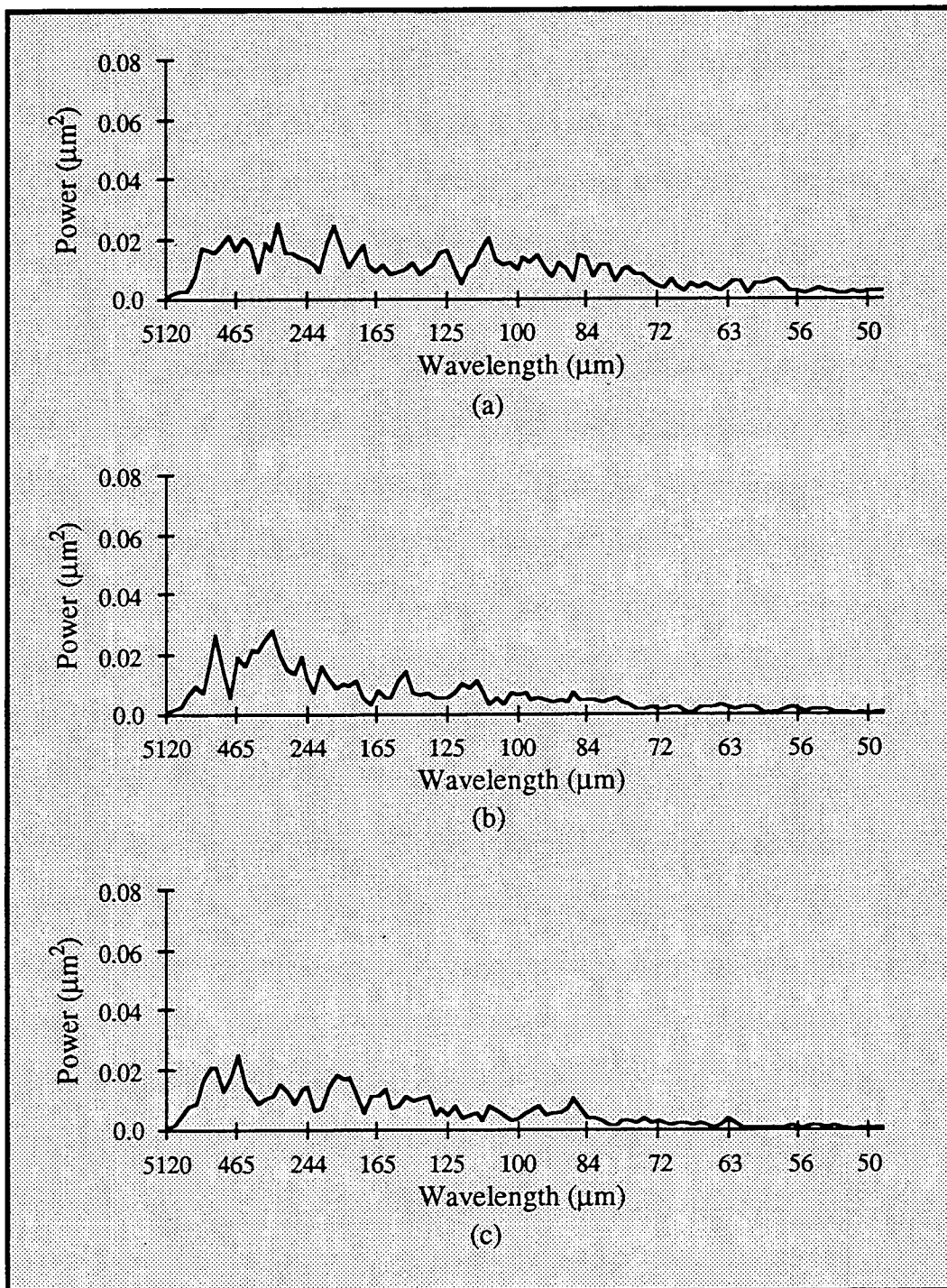


Figure A16: Power Spectra from laboratory coated specimen **EDT 1:**
 (a) uncoated, traces in rolling direction; (b) coated, traces in rolling
 direction; (c) coated, traces in transverse direction.

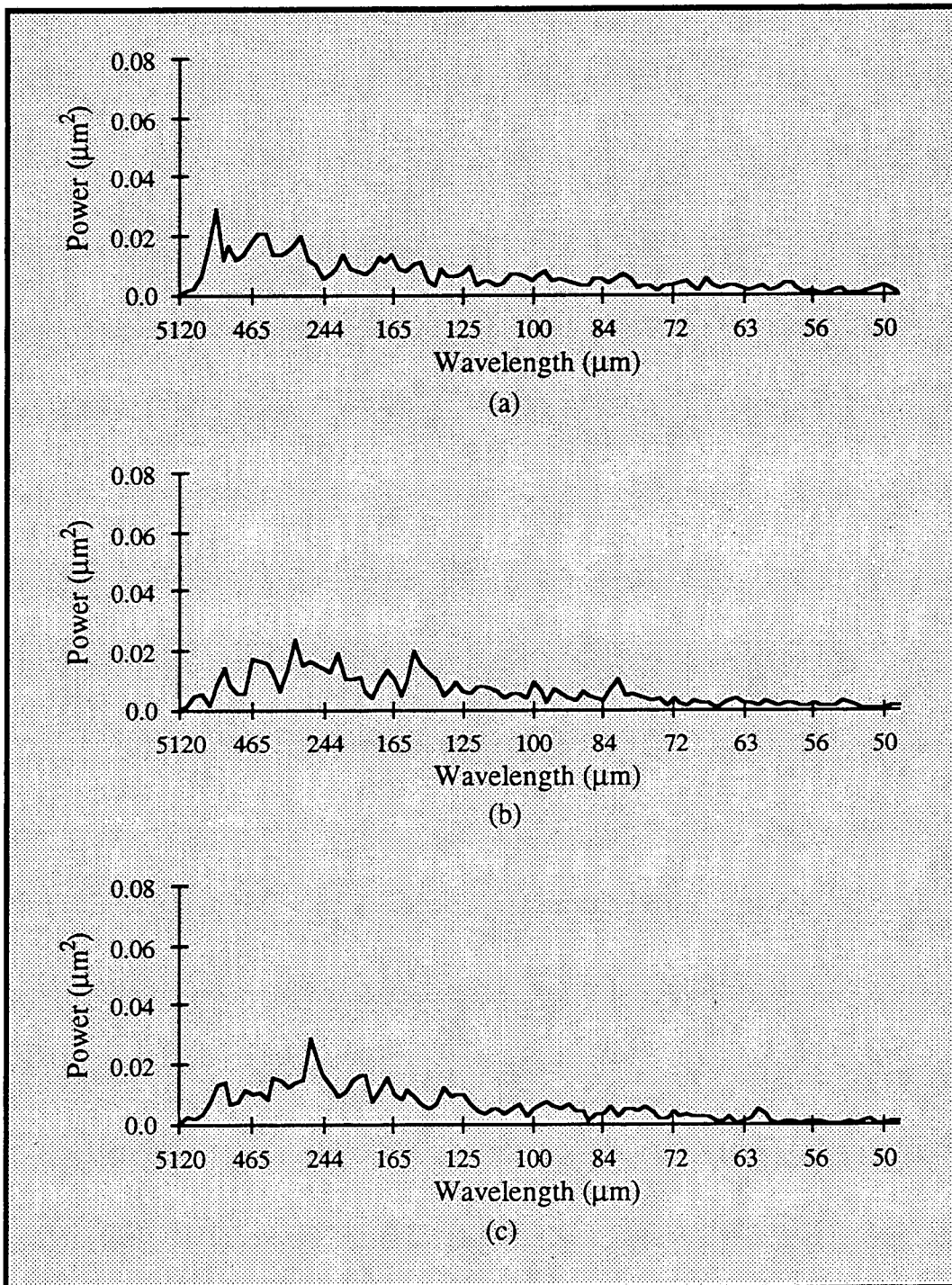


Figure A17: Power Spectra from laboratory coated specimen EDT 2:
 (a) uncoated, traces in rolling direction; (b) coated, traces in rolling
 direction; (c) coated, traces in transverse direction.

APPENDIX B: STATISTICAL PARAMETERS

Most parameters were created to describe single point tooling machined surfaces, where the overall height of the peaks is the dominant feature of interest. Not surprisingly then, the largest number of statistical parameters developed are for describing the roughness of the surface. Each of these parameters emphasizes a different statistical aspect of the measured profile. For example, the maximum peak to valley roughness height, labeled R_y places the emphasis on the largest asperity, which in the case of sheet metal, may simply be a scratch in the surface; the roughness average, or arithmetic average, labeled R_a , minimizes the effect of the largest asperities by averaging the asperities over the entire profile length. Some measurements, such as the ten point height, labeled R_z , were created to find some middle ground between these two extremes by weighting the larger asperities more heavily. R_a is calculated by

$$R_a = \frac{1}{L} \int_{x=0}^{x=L} |y| dx \quad (B1)$$

where L sampling length, and y is the distance of a point on the actual surface to the center line or nominal surface. From a discrete data set this is computed by

$$R_a = \frac{1}{N} \sum_i^N |y_i| \quad (B2)$$

where N is the number of points sampled.

The shape of asperities is not usually one of the specified parameters for most machined engineering surfaces. The two most common parameters used are the Skewness (R_{sk}) and the Kurtosis (R_{ku}). These provide descriptions of how the surface is distributed about the mean, or nominal surface. The R_{sk} describes how the surface is skewed about the mean value (whether the surface tends to have mostly plateaus or mostly valleys). It is given by the formula

$$R_{sk} = \frac{1}{LR_a^{\frac{3}{2}}} \int_{x=0}^{x=L} y^3 dx \quad (B3)$$

and is discretized in the same manner as R_a .

$$R_{sk} = \frac{1}{NR_a^{\frac{3}{2}}} \sum_{i=1}^N y_i^3 \quad (B4)$$

The R_{ku} describes how sharp the distribution is (whether most of the surface is near the mean value or distributed evenly throughout the profile height). It is given in its discrete form by

$$R_{ku} = \frac{1}{NR_a^2} \sum_{i=1}^N y_i^4 \quad (B5)$$

R_a , R_{sk} , and R_{ku} can all be derived from the Amplitude Density Function (ADF), which is defined as the probability density of profile heights. An example of the the calculation of an ADF from a profile is given in Figure A1 and is written mathematically as

$$ADF(y_j) = \frac{\sum_i \Delta L_i}{L \Delta y} \quad (B6)$$

where ΔL_i is the length of the i th portion of the profile within the band of thickness Δy about the j th height value y_j , and L is the total length of the mean profile. In addition, in order to observe how the profile changed as the surface is abraded or worn away, one can also compute the Bearing Area Curve (BAC) which shows what percentage of the nominal surface would support a load if the surface was abraded to a distance above the nominal surface. This combination of parameters, which are defined in terms of the ADF in [40], allows a fairly complete description of the height variation of the surface from one basic

calculation, the *ADF*. However it does not provide a description of the horizontal distribution of peaks on the surface

For measuring the spacing of peaks, the simplest and most common parameter used is the Peak count, labeled P_c , which corresponds to the number of peak/valley pairs per unit length² projecting through a band of width b centered about the mean line [40]. This specification of the band width, b , is arbitrary, and leads to an ambiguity in the meaning of this parameter. This ambiguity suggests the use of a more sophisticated peak distribution description method might be more appropriate for a detailed study of sheet metal surfaces.

Spectral methods offer one possible method of improving this analysis of the spacing of asperities. The topography recorded by the profilometer is recorded by collecting the signal from the stylus at specified distance intervals. If this is plotted as height vs. position, one obtains the standard profile showing where individual points on the surface lie in space. This is referred to as representing the data in the length domain. However, one could also represent these data in the wavelength domain, where the collected set of data is specified as a function of wavelength, not distance. This is merely a different representation of the same data. In order to go back and forth between these two representations one uses the Fourier Transform equations,

$$H(k) = \int_{-\infty}^{\infty} h(x)e^{2\pi ikx} dx \quad (B7)$$

$$h(x) = \int_{-\infty}^{\infty} H(k)e^{-2\pi ikx} dk \quad (B8)$$

In the wavelength domain, the data are represented as a series of sine waves, each having a different wavelength, amplitude and phase. When summed together these sine waves create the profile as plotted in the length domain. Thus, each value of the transformed profile gives the contribution of peaks spaced a given wavelength apart. However, the fourier transform presents these values as complex numbers to include the

effect of phase shifting of the individual sine waves. The real space contribution of the sine wave is described by the power spectrum of the transformed data. The total power of the signal collected is given by

$$Power = \int_{-\infty}^{\infty} |h(x)|^2 dx = \int_{-\infty}^{\infty} |H(k)|^2 dk \quad (B9)$$

and the power in the wavelength interval between l and Dl is given by

$$P_h(k) \equiv |H(k)|^2 + |H(-k)|^2 \quad 0 \leq k < \infty \quad (B10)$$

So in the power spectrum one obtains the contribution to the profile of asperities as a function of their spacing. For discretely sampled data the wavelength range is limited by the smallest wavelength, called the Nyquist wavelength λ_n

$$\lambda_n = 2\Delta l \quad (B11)$$

where Δl is the distance between two consecutive data points, and by the longest wavelength, which is the total sampling length. The median wavelength, λ_m , is the wavelength at which half the power contained in the spectrum is contained in longer wavelengths, and half the power is contained in the shorter wavelengths

$$\sum_{\lambda_{max}}^{\lambda_m} H^2(\lambda) = \sum_{\lambda_m}^{\lambda_n} H^2(\lambda) \quad (B12)$$

For discretely sampled data one can use the fast fourier transform (FFT) to compute the transform of the surface profile and the corresponding power spectrum. Numerous texts on fourier transforms [44,45] and on FFT's [44,46,47] give more detailed discussions of spectral techniques.

From each of the profiles taken from the specimens in this investigation the *ADF* was calculated using a program written By Z. Mei and P. Skarpelos. The R_a , R_{sk} , R_{ku} and *BAC* were then tabulated and averaged for the rolling and transverse directions. The FFT and power spectrum were calculated with the FORTRAN routines in [44]. The

power spectrum for each of the profiles was then combined to give a single, total power spectrum for each of the rolling and the transverse directions. The FORTRAN programs employed are listed in Appendix C.

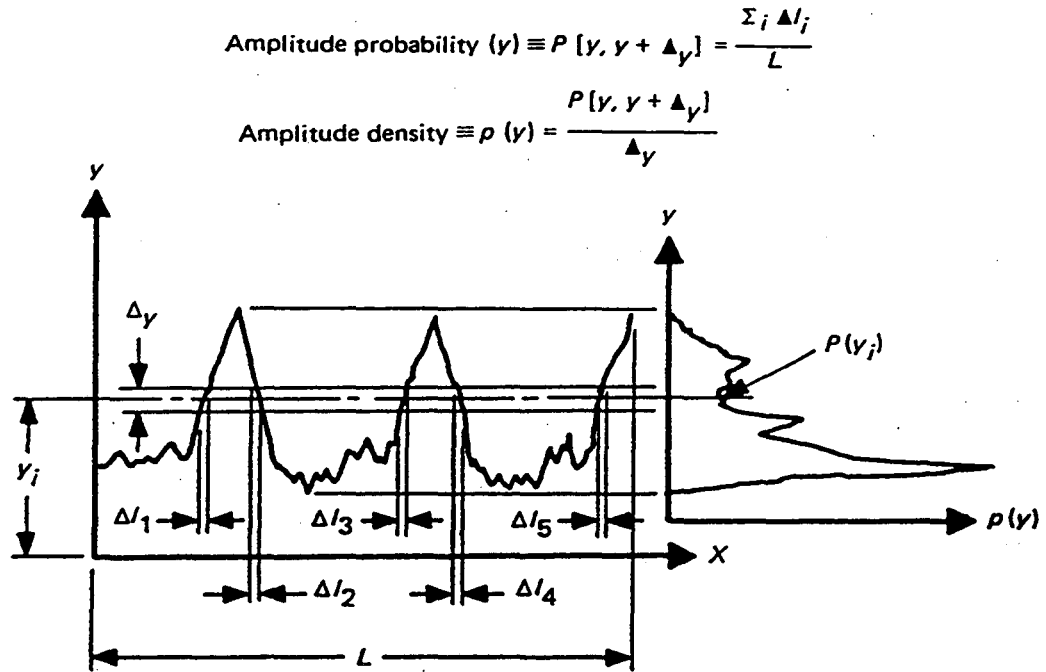


Figure B1: Calculation of the Amplitude Density Function (ADF) from a profile.

APPENDIX C: FORTRAN ALGORITHMS

```

C      Program ANALYSIS
C
PARAMETER(M=512,M2=2*M,PI=3.14159,LMDA=5120)
CHARACTER*8 INAME
CHARACTER*14 IFILE, PWRFILE, BACFILE
REAL*4 DATA, XDATA, P
DIMENSION DATA(M2), XDATA(M2), P(M+1)
C
DO 1 J=1,M+1
  P(J)=0.
1  CONTINUE
  DEN=0.
C
WRITE(5,10)
10  FORMAT(/1H$,ENTER BASE FILENAME ->:)
20  READ(5,20) INAME
  FORMAT(A8)
  PWRFILE = 'A://INAME//.PWR'
  BACFILE = 'A://INAME//.BAC'
  OPEN(2,FILE=PWRFILE,STATUS='UNKNOWN')
  OPEN(3,FILE=BACFILE,STATUS='UNKNOWN')
  DO 999 IEND = 1, 8
    IFILE = 'B://INAME//.00//CHAR(48+IEND)
    WRITE(*,*) 'INPUT FILE: ',IFILE
    OPEN(unit=1, err=1000, file=IFILE, status='OLD', access='DIRECT', recl=8)
C
C      Read the data values from the input file
C
DO 100 J=3,M2+2
  NCOUNT=J-2
  READ(1,REC=J,ERR=101) XDATA(NCOUNT),DATA(NCOUNT)
100  CONTINUE
101  CLOSE(UNIT=1,STATUS='KEEP')
  IF (NCOUNT.LT.M2)THEN
    DO 200 J=NCOUNT+1,M2
      DATA(J)=0.
200  CONTINUE
  ENDIF
C
CALL REGRESS(XDATA,DATA,NCOUNT)
CALL SURF(XDATA,DATA,RA,RQ,RSKEW,RKURT,M2,IEND)
CALL SPCTRM(P,DATA,M,M2,DEN)
999  CONTINUE
1000 CALL FIN(P,DEN,M,LMDA,RA,RQ,RSKEW,RKURT,IEND,INAME)
  CLOSE(2)
  CLOSE(3)
C
C      Tell the user that the analysis is done
C
STOP 'FINISHED ANALYZING FILES.'
END
C
SUBROUTINE FIN(P,DEN,M,LMDA,Ra,Rq,Rskew,Rkurt,IEND,INAME)
C
C      This routine calculates the mean wavelength of the power
C      spectrum produced by SPCTRM and writes the roughness data,
```

```

C      power spectrum and mean wavelength to the file INAME.PWR
C
      DIMENSION P(*)
      REAL ZERO
      CHARACTER*8 INAME
C
      DO 300 J=1,M+1
      P(J)=P(J)/DEN
        IF(J.GT.1)THEN
          SUMY=SUMY+P(J)
        ENDIF
300    CONTINUE
C
      RA = RA/IEND
      RQ = RQ/IEND
      RSKEW = RSKEW/IEND
      RKURT = RKURT/IEND
C
      Now calculate the mean wavelength.
C
      ZERO=0.
      AVG=SUMY*.5
      SUMY=0.
      XREAL=1.0
      DO 400 J=2,M+1
        SUMY=SUMY+P(J)
        NCOUNT=J-1
        IF(SUMY.GE.AVG)THEN
          GOTO 401
        ENDIF
400    CONTINUE
C
      Write data to output file.
C
401    WRITE(2,40)INAME,LMDA/(XREAL*NCOUNT-1.)
      WRITE(2,50)RA,RQ,RSKEW,RKURT
      WRITE(2,30)ZERO,P(1)
      DO 500 I=2,M+1
        WRITE(2,30)LMDA/(XREAL*I-1.),P(I)
500    CONTINUE
30    FORMAT(2(F10.4,2X))
40    FORMAT(2X,A8,' has a mean wavelength of ',F5.0,'microns')
50    FORMAT(2X,'RA = ',F8.4,'RQ = ',F8.4,'RSKEW = ',F8.4,'RKURT = ',F8.4)
      RETURN
      END

```

C

SUBROUTINE SURF(x,yy,Ra,Rq,Rskew,Rkurt,M2,IEND)

C

C

C

C

C

This routine is a reduced version of the program SURFROUF, written by Z. Mei and P. Skarpelos which calculates the four roughness amplitude parameters Ra, calculates the four roughness amplitude parameters Ra, Rq, Rskew, and Rkurt. This is done by calculating the Amplitude Density Function of the profile, from which

C

C

these parameters are derived.

```
DIMENSION X(*),YY(*)
REAL RA,RQ,RSKEW,RKURT
REAL AA,RRMS,SKEWNESS,KURTOSIS
REAL PI(120),ADF(120),BAC(120),Y1(120)
INTEGER ENTER,ENTRY,SN1,SN2,SN11,SN22,SN33
INTEGER SN3,SN4,SN5,SN6,SN7
```

C

C

C

C

Calculate the maximum peak to valley height and break the profile into 50 equal height bands.

```
YYMIN = YY(1)
YYMAX = YY(1)
```

C

```
DO 400 I=2,M2
  IF(YYMIN .GT. YY(I)) YYMIN = YY(I)
  IF(YYMAX .LT. YY(I)) YYMAX = YY(I)
```

400

C

```
CONTINUE
```

```
N = 50
STEP = (YYMAX - YYMIN)/N
```

C

```
S1 = 0.0
DO 500 I = 1,N+1
  Y1(I) = YYMIN + STEP * (I - 1.0)
  X2 = 0.0
  X1 = 0.0
  A1 = Y1(I) - 0.5*STEP
  A2 = Y1(I) + 0.5*STEP
  IF(I .EQ. 1) A1 = YYMIN
  IF(I .EQ. N+1) A2 = YYMAX
  ENTER = 0
  IF (A1 .GT. YY(1)) THEN
    SN1 = 1
  ELSE
    SN1 = -1
  ENDIF
  IF (A2 .GE. YY(1)) THEN
    SN2 = 1
  ELSE
    SN2 = -1
  ENDIF
  SN7 = SN1 * SN2
  IF (SN7 .LT. 0) THEN
    ENTER = 1
    X1 = X(1)
  ENDIF
  BAC(I) = 0.0
  IF (Y1(I) .LE. YY(1)) THEN
```

```

        ENTRY = 1
        XX1 = X(1)
        SN11 = -1
    ELSE
        ENTRY = 0
        SN11 = 1
    ENDIF
C
DO 600 J=2,M2
    IF (Y1(I) .LE. YY(J)) THEN
        SN22 = -1
    ELSE
        SN22 = 1
    ENDIF
    SN33 = SN11 * SN22
    SN11 = SN22
    IF(SN33.LT.0) THEN
        XX2=X(J-1) + (X(J)-X(J-1)) * (Y1(I)-YY(J-1)) / (YY(J)-YY(J-1))
        IF(ENTRY .EQ. 1) THEN
            BAC(I) = BAC(I) + (XX2 - XX1)
            ENTRY = 0
        ELSE
            XX1 = XX2
            ENTRY = 1
        ENDIF
    ENDIF
    IF (J.EQ.M2 .AND. Y1(I).LE.YY(M2).AND. ENTRY.EQ.1) THEN
        XX2 = X(M2)
        BAC(I) = BAC(I) + (XX2 - XX1)
        ENTRY = 0
    ENDIF

```

```

C
    IF(A1 .GT. YY(J)) THEN
        SN3 = 1
    ELSE
        SN3 = -1
    ENDIF
    SN5 = SN1 * SN3
    SN1 = SN3
    IF (SN5 .LT. 0) THEN
        X2=X(J-1) + (X(J) - X(J-1))*(A1 - YY(J-1))/(YY(J)-YY(J-1))
        IF(ENTER .EQ. 1) THEN
            PI(I) = PI(I) + ABS(X2 - X1)
            ENTER = 0
        ELSE
            X1 = X2
            ENTER = 1
        ENDIF
    ENDIF

```

```

C
    IF(A2 .GE. YY(J)) THEN
        SN4 = 1
    ELSE
        SN4 = -1
    ENDIF
    SN6 = SN2 * SN4
    SN2 = SN4
    IF (SN6 .LT. 0) THEN

```

```

X2 = X(J-1) + (X(J)-X(J-1))*(A2-YY(J-1))/(YY(J)-YY(J-1))
IF (ENTER .EQ. 1) THEN
  PI(I) = PI(I) + ABS(X2 -X1)
  ENTER = 0
ELSE
  X1 = X2
  ENTER = 1
ENDIF
600   CONTINUE
      S1 = S1 + PI(I)
500   CONTINUE
C
      S = 0.0
      DO 700 I=1,N+1
        DS = PI(I) * STEP
        IF( (I .EQ. 1) .OR. (I .EQ. N+1) ) DS = 0.5 * DS
        S = S + DS
700   CONTINUE
C
      WRITE(3,10)IEND
      DO 800 I=1,N+1
        ADF(I) = PI(I) / S
        PI(I) = PI(I) / S1
        BAC(I) = BAC(I) / S1
        WRITE(3,20)BAC(I), Y1(I)
800   CONTINUE
10    FORMAT(3X,'BAC #',I1,6X,'HEIGHT')
20    FORMAT(2(3X,F6.3))
C
      AA = 0.0
      RRMS = 0.0
      SKEWNESS = 0.0
      KURTOSIS = 0.0
      DO 1000 I=1,N+1
        DS = Y1(I)
        DS1 = ABS(DS)
        DS2 = DS * DS
        DS3 = DS * DS * DS
        DS4 = DS * DS * DS * DS
        DELTAY = STEP * ADF(I)
        IF ((I.EQ.0) .OR. (I.EQ.N)) DELTAY = 0.5*DELTAY
        AA = AA + DS1 * DELTAY
        RRMS = RRMS + DS2 * DELTAY
        SKEWNESS = SKEWNESS + DS3 * DELTAY
        KURTOSIS = KURTOSIS + DS4 * DELTAY
1000  CONTINUE
C
      RRMS = SQRT(RRMS)
      SKEWNESS = SKEWNESS / RRMS/RRMS/RRMS
      KURTOSIS = KURTOSIS / RRMS/RRMS/RRMS/RRMS
C
      RA = RA + AA
      RQ = RQ + RRMS
      RSKEW = RSKEW + SKEWNESS
      RKURT = RKURT + KURTOSIS
      RETURN
      END

```

```

C
                                SUBROUTINE REGRESS(XDATA,DATA,NCOUNT)
C
C   A routine for calculating a parabolic curve fit to a
C   list of data points.
C
REAL*4 XDATA, DATA
DIMENSION XDATA(*), DATA(*)
INTEGER I, N, NCOUNT, XINCRMNT
REAL X, Y, SX, SY, SX2, SX3, SX4, SXY, SX2Y
REAL A1,A2,A3,DNOMNATR
C
N = 0
SX = 0.0
SY = 0.0
SX2 = 0.0
SXY = 0.0
SX3 = 0.0
SX4 = 0.0
SX2Y = 0.0
XINCRMNT = 1000
DNOMNATR = 0.0
C
DO 100 I = 1, NCOUNT
    N = N + 1
    Y = DATA(I)
    X = XDATA(I)*XINCRMNT
    SX = SX + X
    SY = SY + Y
    SX2 = SX2 + (X**2)
    SXY = SXY + (X*Y)
    SX3 = SX3 + (X**3)
    SX4 = SX4 + (X**4)
    SX2Y = SX2Y + (X**2)*Y
100 CONTINUE
DNOMNATR=SX4*(N*SX2-SX**2)-SX3*(N*SX3-SX2*SX)+SX2*(SX3*SX-SX2**2)
A1 = SX2Y*(N*SX2-SX**2)-SX3*(N*SXY-SX*SY)+SX2*(SXY*SX-SY*SX2)
A1 = A1/DNOMNATR
A2 = SX4*(N*SXY-SY*SX)-SX2Y*(N*SX3-SX2*SX)+SX2*(SX3*SY-SX2*SXY)
A2 = A2/DNOMNATR
A3 = SX4*(SX2*SY-SX*SXY)-SX3*(SX3*SY-SX2*SXY)+SX2Y*(SX3*SX-SX2**2)
A3 = A3/DNOMNATR
WRITE(*,*) ' A1 = ', A1, ' A2 = ', A2, ' A3 = ', A3
DO 200 I = 1, NCOUNT
    XDATA(I) = XDATA(I)*XINCRMNT
    DATA(I) = DATA(I)-A3-A2*XDATA(I)-A1*(XDATA(I)**2)
200 CONTINUE
RETURN
END
C
                                SUBROUTINE SPCTRM(P,DATA,M,M2,DEN)
DIMENSION P(*),DATA(*)
WINDOW(J)=(1.-ABS(((J-1)-FACM)*FACP)) FACM=M-0.5
FACP=1./(M+0.5)
SUMW=0.
DO 11 J=1,M2
SUMW=SUMW+WINDOW(J)**2
11 CONTINUE

```

```

DO 16 J=1,M2
  DATA(J)=DATA(J)*WINDOW(J)
16 CONTINUE
CALL REALFT(DATA,M,1)
P(1)=P(1)+DATA(1)**2
P(M+1)=P(M+1)+DATA(2)**2
DO 17 J=2,M
  J2=J+J
  P(J)=P(J)+DATA(J2)**2+DATA(J2-1)**2
17 CONTINUE
DEN=DEN+M2*SUNW
RETURN
END

C
      SUBROUTINE REALFT(DATA,N,ISIGN)
REAL *8 WR,WI,WPR,WPI,WTEMP,THETA
DIMENSION DATA(*)
THETA=6.28318530717959D0/2.0D0
C1=0.5
IF (ISIGN.EQ.1) THEN
  C2=-0.5
  CALL FOUR1(DATA,N,+1)
ELSE
  C2=0.5
  THETA=-THETA
ENDIF
WPR=-2.0D0*DSIN(0.5D0*THETA)**2
WPI=DSIN(THETA)
WR=1.0D0+WPR
WI=WPI
N2P3=2*N+3
DO 11 I=2,N/2+1
  I1=2*I-1
  I2=I1+1
  I3=N2P3-I2
  I4=I3+1
  WRS=SNGL(WR)
  WIS=SNGL(WI)
  H1R=C1*(DATA(I1)+DATA(I3))
  H1I=C1*(DATA(I2)-DATA(I4))
  H2R=-C2*(DATA(I2)+DATA(I4))
  H2I=C2*(DATA(I1)-DATA(I3))
  DATA(I1)=H1R+WRS*H2R-WIS*H2I
  DATA(I2)=H1I+WRS*H2I+WIS*H2R
  DATA(I3)=H1R-WRS*H2R+WIS*H2I
  DATA(I4)=-H1I+WRS*H2I+WIS*H2R WTEMP=WR
  WR=WR*WPR-WI*WPI+WR
  WI=WI*WPR+WTEMP*WPI+WI
11 CONTINUE
IF (ISIGN.EQ.1) THEN
  HIR=DATA(1)
  DATA(1)=HIR+DATA(2)
  DATA(2)=HIR-DATA(2)
ELSE
  HIR=DATA(1)
  DATA(1)=C1*(HIR+DATA(2))
  DATA(2)=C1*(HIR-DATA(2))
CALL FOUR1(DATA,N,-1)

```

```
ENDIF  
RETURN  
END
```

C

```
                SUBROUTINE FOUR1(DATA,NN,ISIGN)  
REAL*8 WR,WI,WPR,WPI,WTEMP,THETA  
DIMENSION DATA(*)  
N=2*NN  
J=1  
DO 11 I=1,N,2  
    IF(J.GT.I)THEN  
        TEMPR=DATA(J)  
        TEMPI=DATA(J+1)  
        DATA(J)=DATA(I)  
        DATA(J+1)=DATA(I+1)  
        DATA(I)=TEMPR  
        DATA(I+1)=TEMPI  
    ENDIF  
    M=N/2  
1    IF ((M.GE.2).AND.(J.GT.M)) THEN  
        J=J-M  
        M=M/2  
        GO TO 1  
    ENDIF  
    J=J+M  
11   CONTINUE  
    MMAX=2  
2    IF (N.GT.MMAX) THEN  
1    STEP=2*MMAX  
        THETA=6.28318530717959D0/(ISIGN*MMAX)  
        WPR=-2.D0*DSIN(0.5D0*THETA)**2  
        WPI=DSIN(THETA)  
        WR=1.D0  
        WI=0.D0  
        DO 13 M=1,MMAX,2  
            DO 12 I=M,N,ISTEP  
                J=I+MMAX  
                TEMPR=SNGL(WR)*DATA(J)-SNGL(WI)*DATA(J+1)  
                TEMPI=SNGL(WR)*DATA(J+1)+SNGL(WI)*DATA(J)  
                DATA(J)=DATA(I)-TEMPR  
                DATA(J+1)=DATA(I+1)-TEMPI  
                DATA(I)=DATA(I)+TEMPR  
                DATA(I+1)=DATA(I+1)+TEMPI  
12            CONTINUE  
                WTEMP=WR  
                WR=WR*WPR-WI*WPI+WR  
                WI=WI*WPR+WTEMP*WPI+WI  
13            CONTINUE  
                MMAX=ISTEP  
                GO TO 2  
    ENDIF  
    RETURN  
    END
```

LAWRENCE BERKELEY LABORATORY
UNIVERSITY OF CALIFORNIA
TECHNICAL INFORMATION DEPARTMENT
BERKELEY, CALIFORNIA 94720

AAS268



LBL Libraries